Modelling and Optimising the Performance of Graphene Oxide-Cu2SnS3-Polyaniline nanocomposite as an Adsorbent for Mercury Ion Removal

Modelling and Optimising the Performance of Graphene Oxide-Cu_2SnS_3-Polyaniline nanocomposite as an Adsorbent for Mercury Ion Removal

Sara Enferadi[1], Mohammad Eftekhari[2], Mohammad Gheibi[3], Nikoo Nabizadeh Moghaddam[1], Stanislaw Wacławek[3], Kourosh Behzadian[4]*

[1]Department of Chemistry, Faculty of Sciences, Ferdowsi University of Mashhad, Mashhad, Iran

[2]Department of Chemistry, Faculty of Sciences, University of Neyshabur, Neyshabur, Iran

[3]Institute for Nanomaterials, Advanced Technologies and Innovation, Technical University of Liberec, Studentská 1402/2, 461 17 Liberec, Czech Republic

[4] School of Computing and Engineering, University of West London, St Mary's Rd, London, W5 5RF, UK

E-mail: kourosh.behzadian@uwl.ac.uk

Abstract

Finding a cost-effective, efficient and environmentally friendly technique for removal of mercury ion (Hg^{2+}) in water and wastewater can be a challenge task. This paper presents a novel and efficient adsorbent known as the Graphene oxide-Cu_2SnS_3-Polyaniline (GO-CTS-PANI) nanocomposite, which was synthesised and utilised to eliminate mercury ions (Hg^{2+}) from water samples. The soft–soft interaction between Hg^{2+} and sulfur atoms besides chelating interaction between -N and Hg^{2+} and also electrostatic interaction are the main mechanisms for Hg^{2+} adsorption onto the GO-CTS-PANI adsorbent. Various characterisation techniques, including Fourier transform infrared spectrophotometry (FT-IR), Field Emission Scanning Electron Microscopy (FESEM), Energy-dispersive X-ray spectroscopy (EDX), Elemental Mapping analysis, and X-ray diffraction analysis (XRD), were employed to analyse the adsorbent. The Box-Behnken method, utilising Design Expert Version 7.0.0, was employed to optimise the crucial factors influencing the adsorption process, such as pH, adsorbent quantity, and contact time. The results indicated that the most efficient adsorption occurred at pH 6.5,

with 12 mg of GO-CTS-PANI adsorbent, and a 30-minute contact time, achieving a maximum removal rate of 95% for 50 mg/L Hg^{2+} ions. The study also explored the isotherm and kinetics of the adsorption process, revealing that adsorption took place in sequential layers (Freundlich isotherm) and was followed by a physical interaction between the adsorbent and the adsorbate. The pseudo second-order kinetic equation proved to be a suitable model for interpreting the kinetic data. Furthermore, Response Surface Methodology (RSM) analysis indicated that pH was the most influential parameter in enhancing adsorption efficiency. In addition to traditional models, this study employed artificial intelligence methods, such as the Random Forest algorithm, to enhance the prediction of adsorption process efficiency. The findings demonstrated that the Random Forest algorithm exhibited high accuracy, achieving a correlation coefficient of 0.98. Overall, this research underscores the potential of the GO-CTS-PANI composite for effectively removing Hg^{2+} ions from water resources.

Keywords: *Adsorption, Artificial Intelligence, Graphene oxide-Cu_2SnS_3-PANI, Mercury ion, Response Surface Methodology*

Introduction

In the present era, addressing heavy metal pollution poses a significant challenge to environmental preservation (Briffa et al., 2020). One such hazardous metal is mercury ion (Hg^{2+}), which exhibits toxicity even at low concentrations, leading to detrimental impacts on various bodily systems, including the nervous, digestive, immune, respiratory, and renal systems (Raj and Maiti 2019; Rice et al., 2014). The presence of Hg^{2+} in the environment is primarily attributed to human activities such as gold mining, alloy manufacturing, smelting, electricity and pesticide production, paint manufacturing, and waste incineration (Tchounwou et al., 2003; Mbanga et al., 2019; Streets et al., 2011). It infiltrates water resources through processes like atmospheric deposition, surface runoff, and direct discharge from industries and sewage treatment facilities. Once in water, Hg^{2+} can be converted into methylmercury by

bacteria, a highly toxic form of the element. Methylmercury accumulates in the food chain, particularly in aquatic organisms like fish, resulting in biomagnification and posing a health risk to humans when consumed (Global Mercury Assessment 2018; Yu et al., 2016). According to the recent Global Mercury Assessment, approximately 2000-2500 tonnes of mercury are released into the atmosphere, water, and soil each year (Global Mercury Assessment 2018). Consequently, the removal of Hg^{2+} from environmental water samples is of paramount importance.

Various techniques, including adsorption (Yu et al., 2016; Santana et al., 2016), membrane filtration (Albatrni et al., 2021; Yan et al., 2021), ion exchange (Han et al., 2020), and coagulation (Vasudevan et al., 2012), have been employed for this purpose. Among these, adsorption is the most commonly used method due to its inherent advantages, including the ease of preparing synthetic and natural adsorbents, relatively low cost, and high removal efficiency (Saadati et al., 2023; Rezazadeh et al., 2022; Wei et al., 2018; Li et al., 2014; Lei et al., 2014).

Graphene oxide (GO) is an oxidised form of graphene featuring oxygen-based functional groups that render it hydrophilic and readily dispersible in aqueous solutions. Its surface can be chemically or physically modified with various functional groups, making it suitable for a range of applications, including water treatment (Arshad et al., 2019; Amini-Fazl et al., 2021). Ternary Cu_2SnS_3 (CTS) is an environmentally friendly material with optoelectronic properties, well-suited for photoelectrochemical applications (Jathar et al., 2021). It also contains readily available elements, making it a cost-effective material (Berg et al., 2012). Furthermore, the presence of sulfur atoms (soft base) in CTS makes it an effective adsorbent for toxic soft heavy metals like Hg^{2+} (Velempini and Pillay 2019). Thus, the main purpose of the proposed method is to synthesise and characterise of GO-CTS-PANI nanocomposite to be used as an adsorbent that would maximise the efficiency of the removal of Hg^{2+} ions from water sample. This can

be achieved by synthesising CTS nanoplates and then its characterisation to modify GO followed by modification with PANI. Since CTS nanoplates have Sulphur atoms in its structure, it could be served as a suitable adsorbent for the removal of Hg^{2+} as a very toxic ion. Hence, this study first aims to synthesise GO nanosheets using the Hummer method and modify them with CTS nanoplates and polyaniline (PANI) to create the GO-CTS-PANI nanocomposite. The synthesised adsorbent undergoes thorough characterisation using various techniques, including Fourier transform infrared spectrophotometry (FT-IR), Field Emission Scanning Electron Microscopy (FESEM), Energy-dispersive X-ray spectroscopy (EDX), Elemental Mapping analysis, and X-ray diffraction analysis (XRD). To determine the optimal conditions for achieving the maximum removal percentage (RP), the Box-Behnken experimental design is employed, and various isotherm and kinetic models are assessed and interpreted. Finally, both the Box-Behnken method and Random Forest algorithms are utilised for optimising and predicting the performance of the adsorption system, respectively.

Methodology

This study is divided to different parts including experimental and numerical efforts which are demonstrated in **Figure 1**. According to the scheme, it can be found that experimental practices containing the characterisations and adsorption application process. Likewise, the numerical parts including classical computations for adsorption mechanism analysis, optimisation by Response Surface Methodology, and Machine Learning calculations.

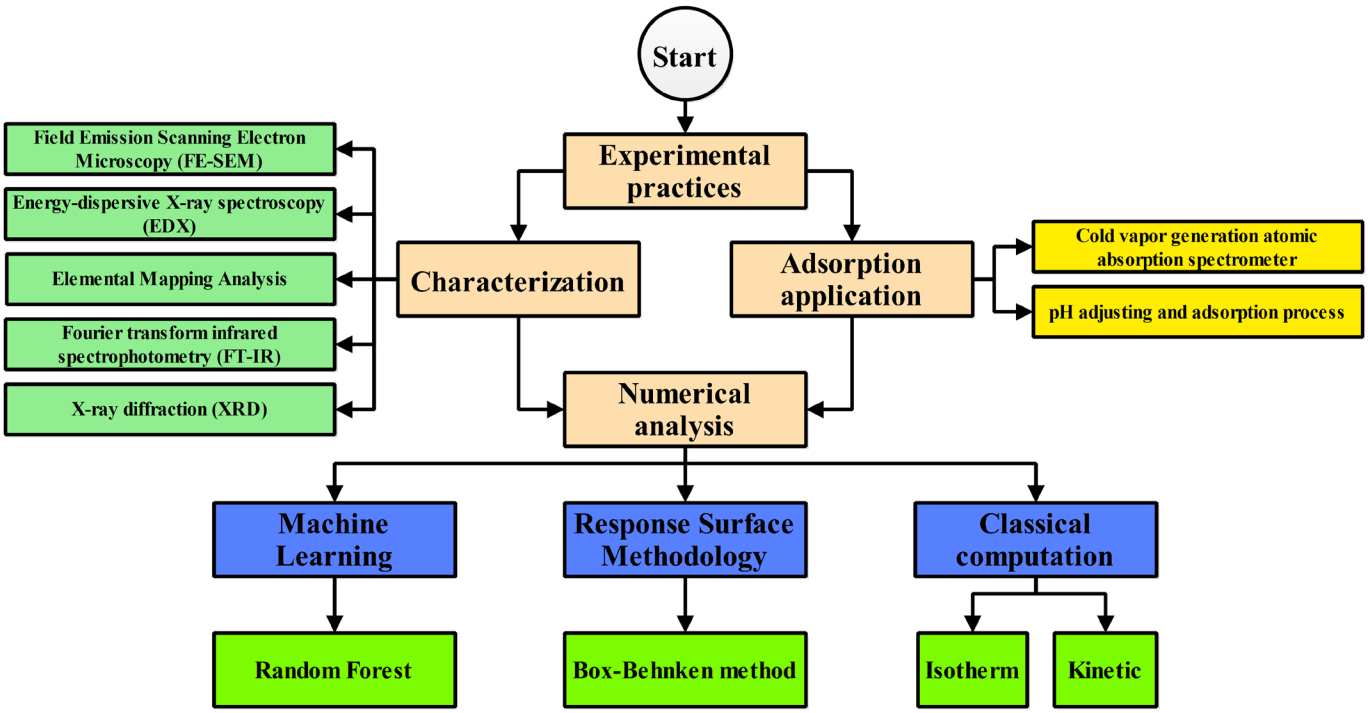

Figure 1. The research roadmap of this study.

Instruments

FE-SEM, EDX, and Elemental Mapping Analysis were conducted using a BRNO-Mira3 LMU device manufactured by TESCAN in the Czech Republic. FT-IR analysis was performed with an AVATAR 370 spectrometer from the US, and XRD analysis utilized a D8-Advance Bruker Cu Kα1 instrument, also from the US. To determine the concentration of Hg^{2+}, a cold vapor generation atomic absorption spectrometer (CV-AAS, Perkin Elmer Analyst 700, USA) equipped with a Hg hollow cathode lamp emitting at 253.7 nm was employed. pH adjustments were made with a Metrohm 827 pH-meter from Switzerland, and the separation of the

adsorbent from the solution was accomplished using an Andreas Hettich D72 centrifuge instrument from Germany.

Reagents

The following reagents and chemicals were used in the experiment: Mercury nitrate monohydrate (Merck, Germany) to prepare a 1000 mg L^{-1} Hg^{2+} solution, Graphite, $Cu(NO_3)_2.3H_2O$, $SnCl_2.2H_2O$, thiourea, aniline, ammonium persulfate, H_2SO_4 (98.0%), $KMnO_4$ (99.0%), H_2O_2 (30%), sodium borohydride ($NaBH_4$, 99.0%) and HNO_3 (65.0%). All of these chemicals and reagents were also provided by Merck (Germany).

Synthesis of GO-CTS-PANI nano-composite

Synthesis of GO and CTS nanoplates

GO was synthesised using the Hummers method as described in **Figure 2** (Rezazadeh et al., 2022b). On the other hand, CTS was synthesised according to the following procedure: 0.241 g $Cu(NO_3)_2.3H_2O$ and 0.114 g $SnCl_2.2H_2O$ were dissolved in 50 ml deionised water. Then 0.114 g thiourea was added to the mixture which causes to the formation of milky mixture. It was then stirred for 30 minutes and autoclaved at 180°C for 8 hours in a 100 mL Teflon-lined stainless-steel autoclave. The resulting CTS nanoplates washed with deionised water three times and dried overnight at 70 °C (Wang et al., 2017).

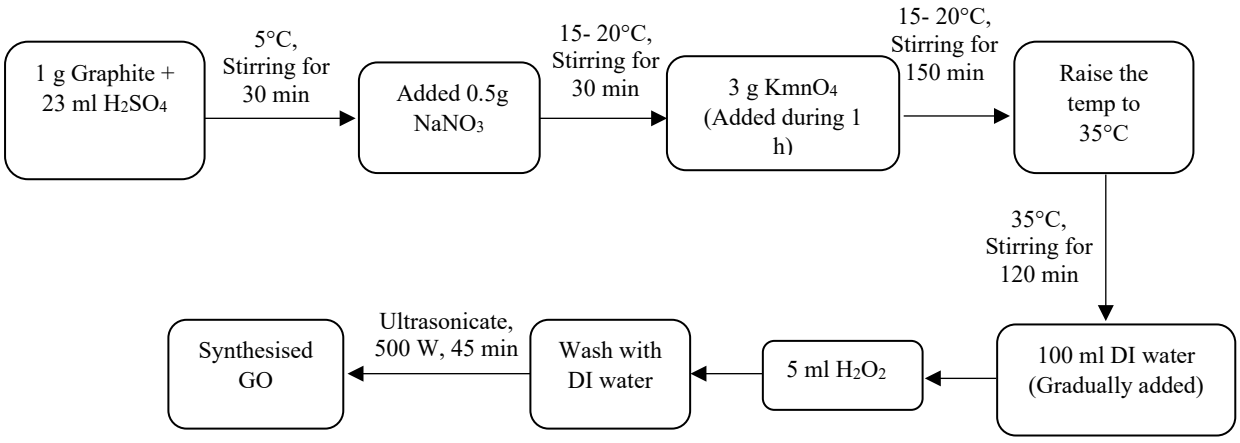

Figure 2. Synthetic route of GO in this study

Synthesise of GO-CTS nanocomposite

To prepare the GO-CTS nanocomposite; 0.5 g of the synthesised GO in 100 ml deionised water (mixture 1) and 0.15g of CTS nanoplates in 50ml deionised water (mixture 2) were separately ultrasonicated for 45 minutes to obtain uniform mixtures. By addition of mixture 2 into the mixture 1, it was stirred for 6 hours at 400 rpm. The synthesised GO-CTS nanocomposite washed with deionised water three times and dried at 60 °C overnight.

Synthesise of GO-CTS-PANI nanocomposite

In a solution containing 0.5 g of GO-CTS in 100 ml deionised water, 500 µL of aniline (in its monomeric form) was introduced and stirred for a duration of 10 minutes. Following this, 10 mL of a 1% ammonium persulfate solution was gradually incorporated into the mixture and stirred for a total of 10 h at 400 rpm. The resulting composite, known as GO-CTS-PANI nanocomposite, underwent multiple washes with deionized water and was subsequently dried overnight at 60 °C.

Removal procedure

In a test solution with an initial Hg^{2+} concentration of 50 mg L^{-1} at a pH of 6.5, 15 mg of GO-CTS-PANI was introduced, and the blend was agitated for a duration of 45 minutes. Subsequent to centrifugation for 5 min at 5000 rpm, the final concentration of Hg^{2+} at equilibrium was determined using CV-AAS. The removal percentage (RP) and the adsorption capacity (qe) were computed utilizing Equation (1) and (2), respectively.

$$RP = \frac{(C_0 - C_e)}{C_O} \times 100 \quad (1)$$

$$q_e = \frac{(C_0 - C_e) \times V}{m} \quad (2)$$

where C_e and C_0 = equilibrium and initial concentration of Hg^{2+} in mg per litre, respectively. V= Sample volume in Lit, m= Adsorbent dosage in grams.

Optimisation process

In order to enhance the efficiency of the experiment, a Box-Behnken design was utilized through Design Expert Version 7.0.0. The Box-Behnken design belongs to response surface methodology, which constructs a second-order polynomial equation to depict the connection between the influencing factors and the response variable. These influencing factors, encompassing pH, the quantity of adsorbent (M), and contact duration, were modified across three levels, resulting in a total of 15 experimental trials. The mathematical model derived from the Box-Behnken design is represented by Equation 3, as detailed in the work of Eftekhari et al. (2020).

$$Y = \beta0 + \beta1X1 + \beta2X2 + \beta3X3 + \beta11X1^2 + \beta22X2^2 + \beta33X3^2 + \beta12X1X2 + \beta13X1X3 + \beta23X2X3 \quad (3)$$

Herein, Y represents the response variable, β0 is the constant coefficient, β1-β3 are the linear coefficients and β11, β22, and β33 are the quadratic coefficients. Moreover, β12, β13, and β23 are the interaction coefficients.

In the optimisation process, the model performance is examined by desirability functions based on the most important features. The function involves transforming multiple response variables into a single scalar value between 0 and 1, where a value of 1 indicates the optimal condition for all response variables, and a value of 0 indicates the worst condition. The desirability function can be described as the result of multiplying individual desirability functions, with each individual function signifying the degree of desirability for a specific response variable. The allocation of weights for these functions is determined by considering the relative significance of each response variable in relation to the overall performance of the system, as outlined in the work by Eftekhari et al. (2020).

Classical computations

The two-parameter isothermal equations represent mathematical formulas used to describe how adsorption capacity behaves under constant temperature conditions. Meanwhile, the three-parameter isothermal equations share similarities with the two-parameter equations but introduce an additional parameter to better capture the characteristics of the adsorption process (Eftekhari et al., 2020). Initially, the data is analysed using the two-parameter isotherm equations. If both the Langmuir and Freundlich models demonstrate similar performance, then the three-parameter equations are employed to precisely predict the adsorption mechanism (Eftekhari et al., 2020). In this research, both two-parameter models (Dubinin-Radushkevich, Temkin, Langmuir, and Freundlich) and three-parameter models (Toth, Khan, and Sips) are utilized to assess the adsorption mechanism. Furthermore, to evaluate the dynamic behavior of the adsorption process, several kinetic equations are applied (Eftekhari et al., 2020).

Machine Learning calculations

In this current research, the Random Forest (RF) algorithm was employed to predict the removal percentage based on various influential factors, including pH, the quantity of adsorbent, and contact time. The RF algorithm is a machine learning technique that creates numerous decision trees during the training phase and outputs either the mode of the classes (for classification tasks) or the mean prediction (for regression tasks) from the individual trees. In this specific study, the RF algorithm was trained using a dataset comprising known removal percentages and their corresponding influential factors. Additionally, to ensure the accuracy and robustness of the model, the optimal K-fold value was fine-tuned (Eftekhari et al., 2021). The K-fold technique is a method for validating a model, involving the division of the dataset into K equally sized subsets or folds. The model is trained on K-1 folds and tested on the remaining fold, with this process repeated K times. The model's performance is then averaged across the K folds to provide an estimate of its accuracy. In this study, the optimal K value was

194 determined by adjusting the parameter through a grid search approach (Eftekhari et al., 2021).
195 The mathematical representation of the RF algorithm can be found in Equation 4.
196 Given a training set T = {(x1,y1), (x2,y2),..., (xn,yn)} (4)
197 In the context of this equation where "xi" represents the influential factors and "yi" stands for
198 the corresponding removal percentage, the RF algorithm generates a diverse set of decision
199 trees denoted as "Ti" by employing bootstrap aggregating, commonly referred to as "bagging,"
200 on the training dataset "T" (Eftekhari et al., 2021). The result produced by the RF algorithm
201 corresponds to the class that emerges as the mode among the classes (for classification tasks)
202 or the mean prediction (for regression tasks) from the individual decision trees. All
203 computational tasks and model training were carried out using WEKA 3.9.

204 **Results and Discussion**

205 **Characterisation of CTS nanoplates and GO-CTS-PANI composite**

206 The CTS nanoplates were synthesised and characterised using XRD, FESEM, and EDX
207 analysis. FESEM images of the synthesised CTS nanoplates are shown in **Figure 3**, while the
208 EDX spectrum presented in **Figure 4** confirms the high purity of CTS nanoplates with peaks
209 corresponding to Cu (0.93 and 8.04 keV), Sn (3.44 keV) and S (2.31 keV). XRD patterns of
210 the synthesised CTS nanoplates are illustrated in **Figure 5**, which shows major diffraction
211 peaks appearing at $2\Theta = 28.5^{\circ}$, 32.8°, 47.5°, 56.4° and 68.6°. These peaks correspond to (111),
212 (200), (220), (311) and (400) of CTS (JCPDS no. 89-2877), indicating the CTS nanoplates
213 possess a cubic phase (Zaman and Poolla 2020).

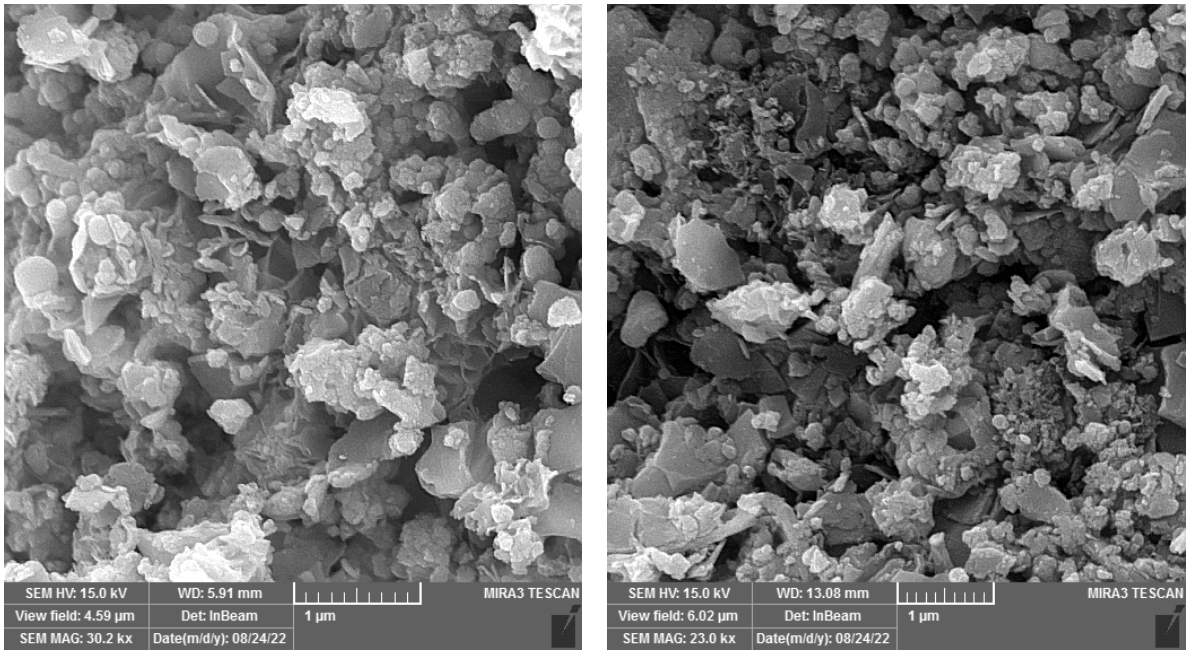

(a) (b)

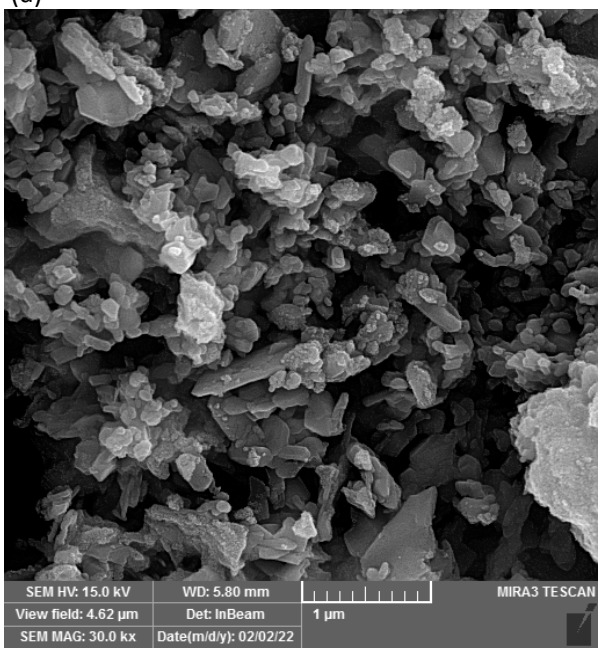

(c)

Figure 3. FESEM images of CTS nanoplates (a-c)

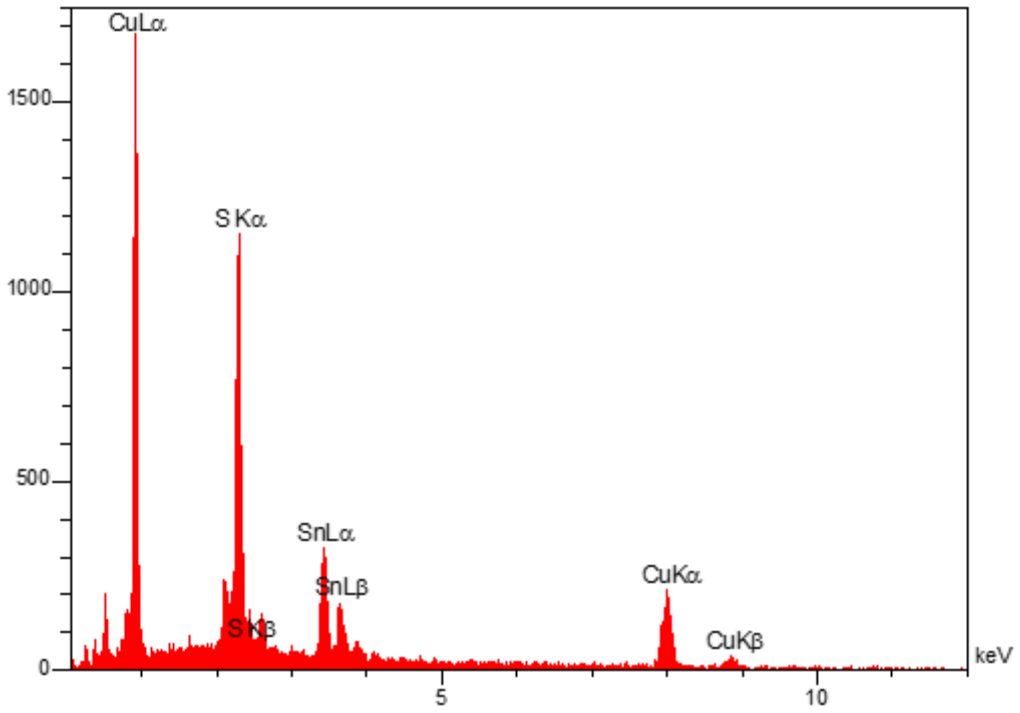

Figure 4. EDX analysis of CTS nanoplates

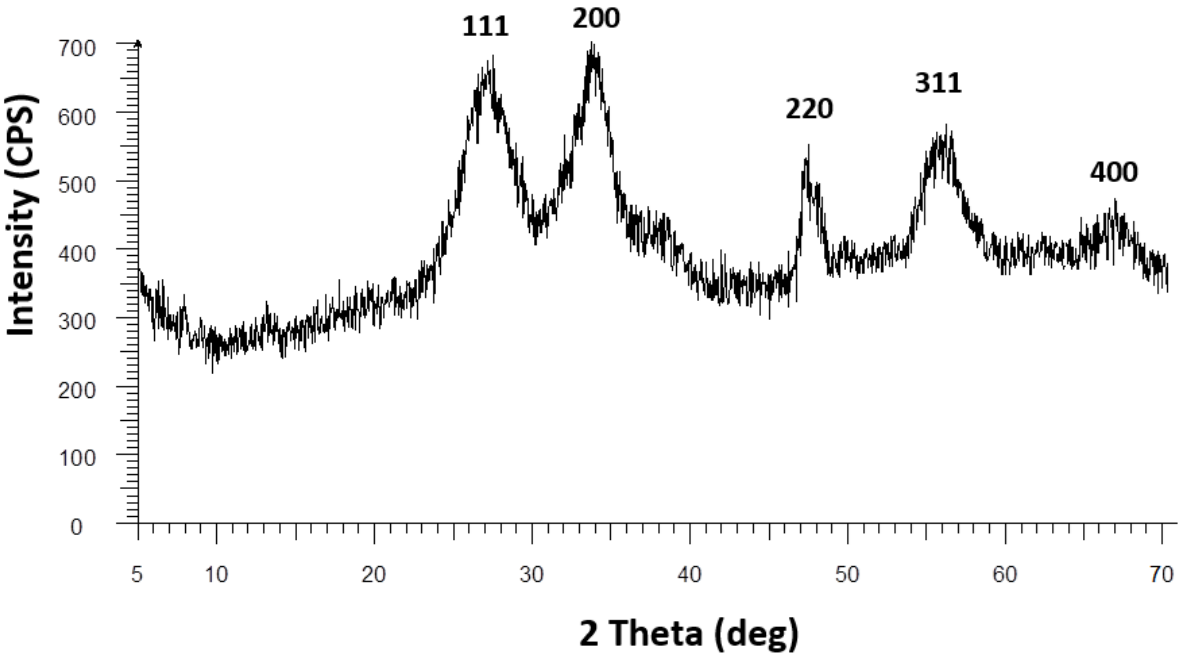

Figure 5. XRD spectrum of CTS nanoplates

Figure 6 presents FESEM images of GO-CTS-PANI composite, which indicates that GO nanosheets are occupied by CTS nanoplates and PANI. EDX analysis of the composite in **Figure 7** also shows the presence of N and O groups at 0.39 and 0.52 eV, respectively, which are attributed to PANI and GO in the synthesised composite.

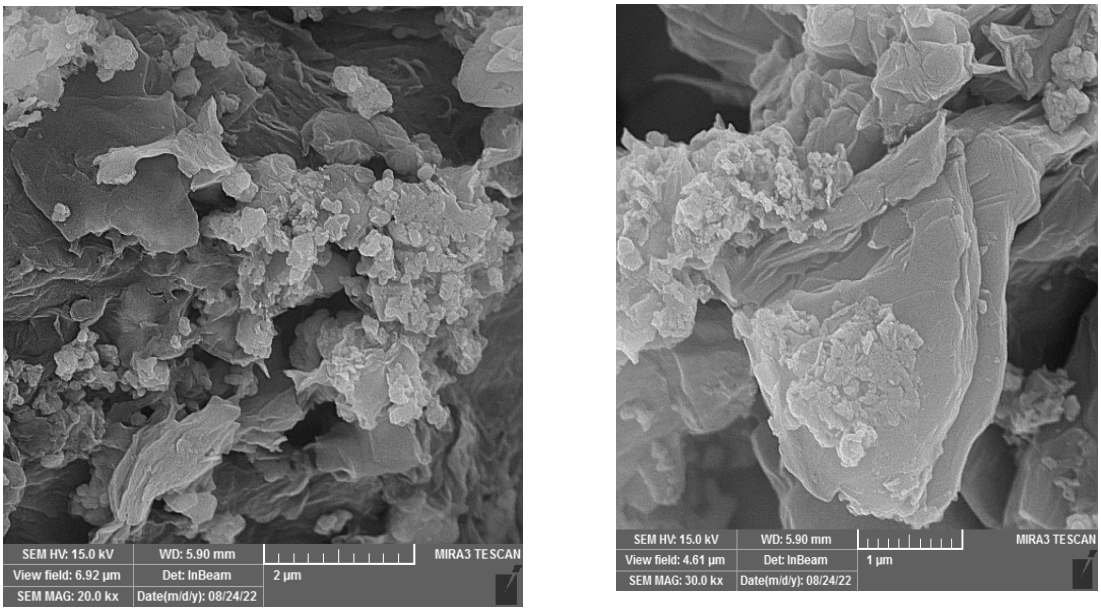

(a) (b)

(c)

Figure 6. FESEM images of GO-CTS-PANI nanocomposite

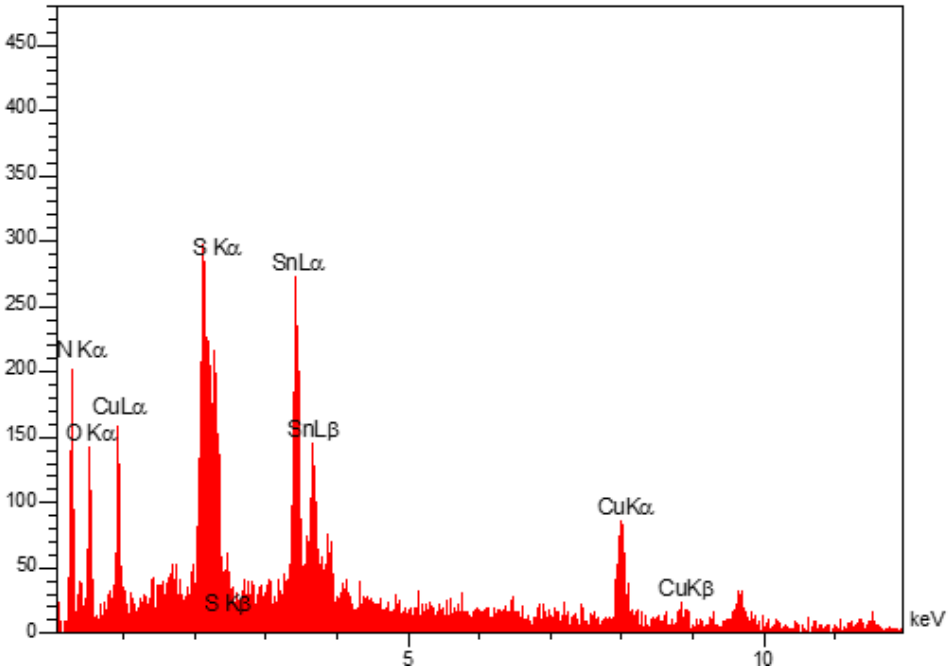

Figure 7. EDX analysis of GO-CTS-PANI composite

The GO-CTS-PANI composite was analysed using XRD in **Figure 8**. The analysis revealed clear appearance of the main peaks of CTS nanoplates in the spectrum. In addition, two peaks of GO at 2Θ = 11.6° and 42.5° correspond to (001) and (101), respectively (Shabani-Nooshabadi and Zahedi 2019) while a broad peak at 2Θ=20° corresponds to (100) and attributed to PANI (Liu et al., 2018).

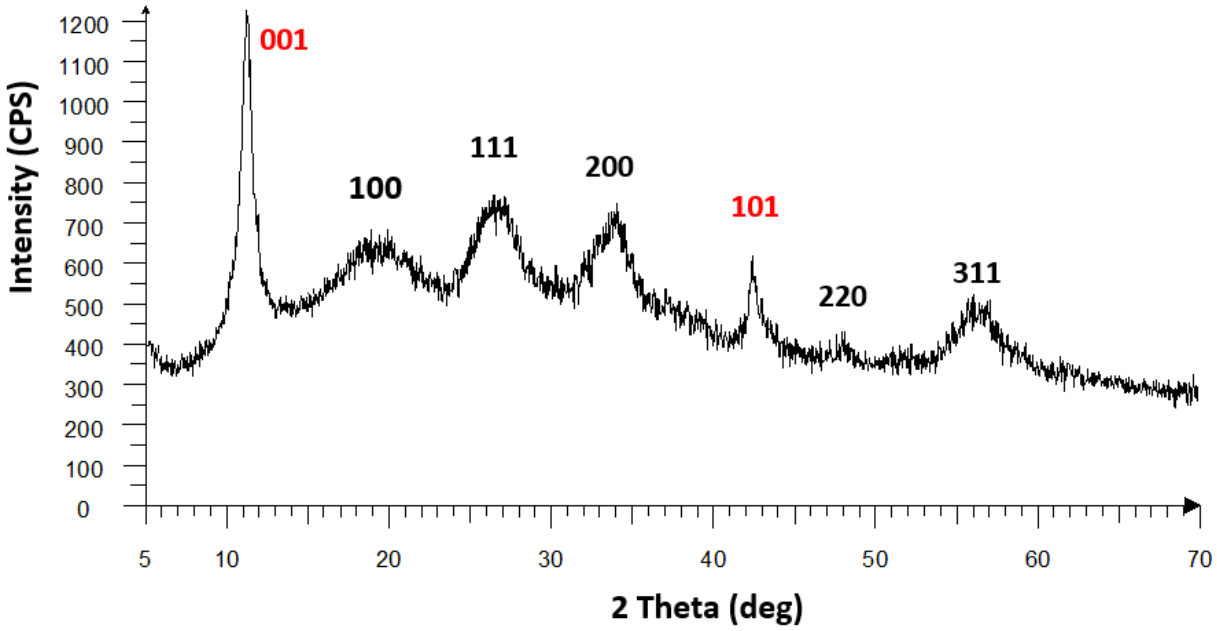

Figure 8. XRD spectrum of GO-CTS-PANI nanocomposite

MAP analysis was conducted on GO-CTS-PANI nanocomposite, and the results (**Figure 9a-e**) revealed that C (7a), Cu (7b), N(7c), O(7d), S(7e) and Sn (7f) are the main components of the synthesised GO-CTS-PANI nanocomposite.

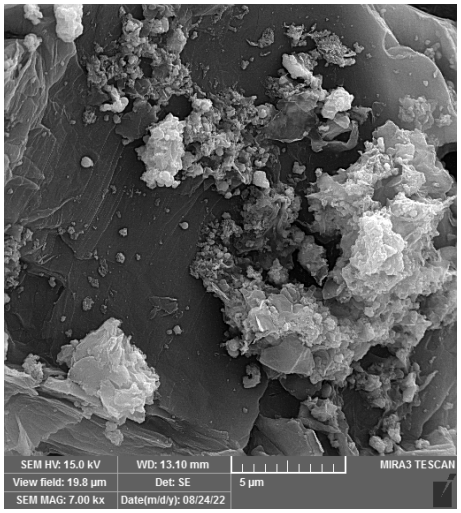

(a)

(b)

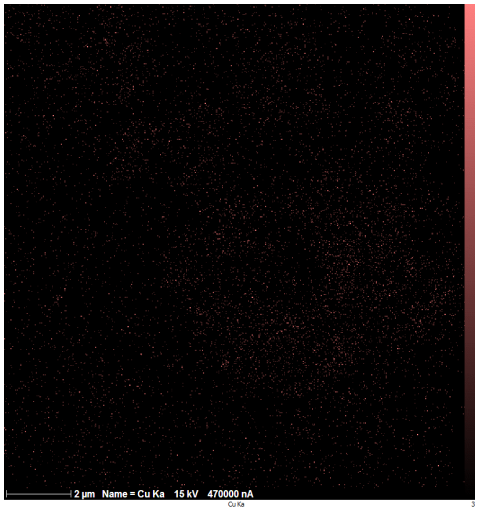

(c)

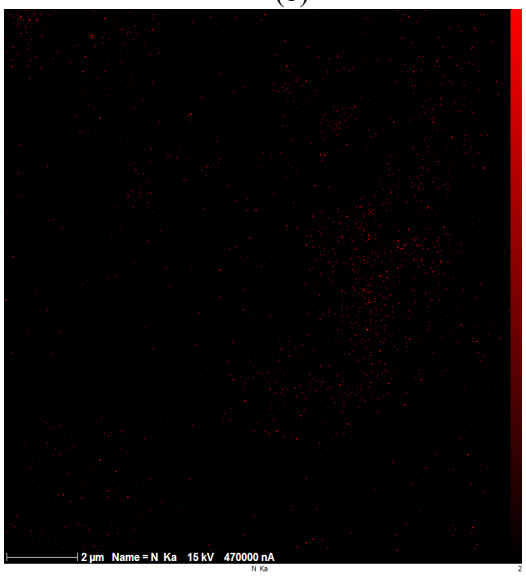

(d)

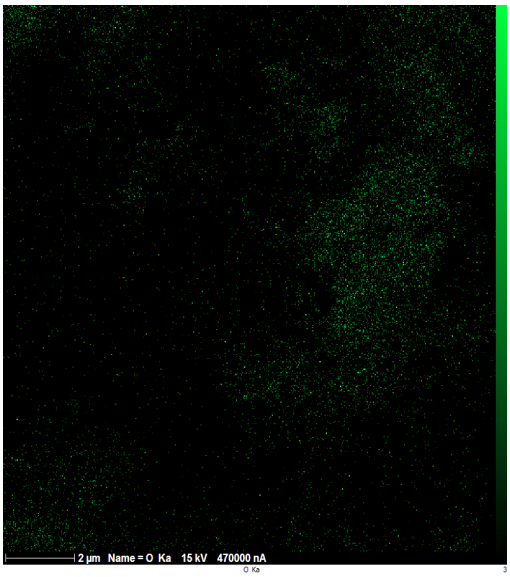

(e)

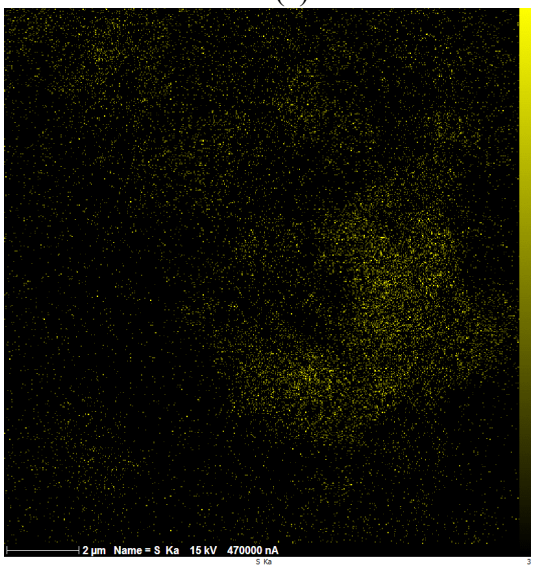

(f)

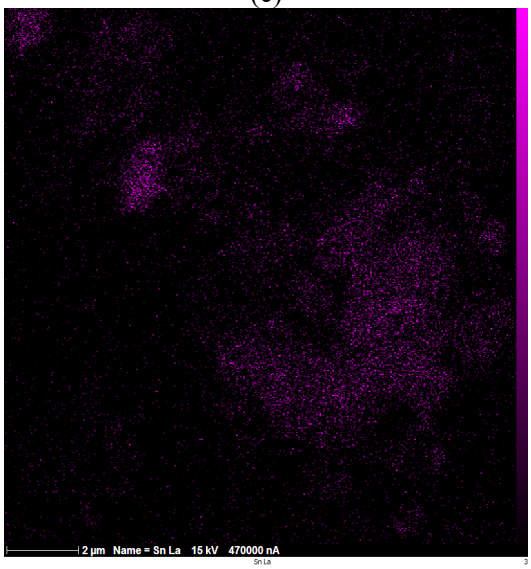

(g)

Figure 9. MAP elemental analysis of GO-CTS-PANI; distribution of mapping zone in SEM image (a) C (b), Cu (c), N(d), O(e), S(f) and Sn (g) (a-f images).

Finally, the FT-IR spectra of GO-CTS-PANI composite and CTS nanoplates are presented in **Figure 10**. The CTS spectrum shows a sharp peak at 500-750 cm^{-1} that is related to the vibration of Cu-S, Sn-S bonds. The band at 1630 cm^{-1} is due to the O-H bending of water molecules and a peak appeared at 1130 cm^{-1} could be attributed to the stretching vibration of C-N band of thiourea in the structure of CTS nanoplates. The FT-IR spectrum of GO-CTS-PANI shows the peaks at 3300 cm^{-1} (stretching of N-H, O–H), 1050 cm^{-1} (C–O of hydroxyl group), 1730 cm^{-1} (C=O) and 1650 cm^{-1} (C=C). Moreover, the intense peak of Cu-S and Sn-S (at 500-750 cm^{-1}) in CTS nanoplates is reduced after modification by GO-PANI.

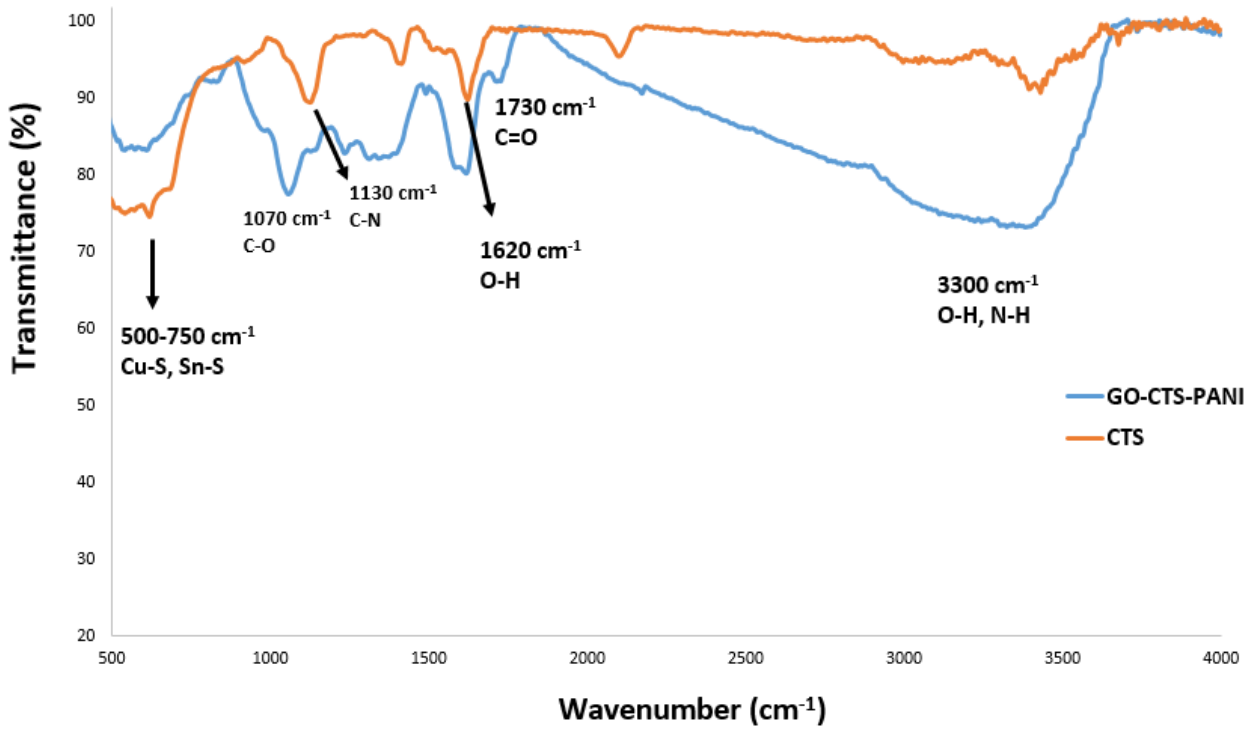

Figure 10. FT-IR spectrum of the synthesised CTS nanoplates and GO-CTS-PANI

Optimisation of parameters

To optimise effective features including pH, adsorbent amount (M), and contact time, Box-Behnken method was applied using Design Expert Version 7.0.0 for 50 mg L^{-1} Hg^{2+} ion. The

range of each parameter in the Design of Experiments (DOE) as well as the statistical analysis outcomes of experiments are presented in Table 1. The responses obtained from the experiments are distributed between 36% and 95%. Also, the model follows polynomial and quadratic equation for fitting effective features as per removal percentage of Hg^{2+}. Likewise, according to Table 1, it can be concluded that there is spread distribution of Hg^{2+} ion purification from water samples in different conditions of adsorption operation process. Therefore, finding the optimum condition will be valuable in viewpoints of water treatment efficiency.

Table 1. The limitations of DOE in this study

Factor	Name	Units	Type	Low Actual	High Actual	Low Coded	High Coded	Mean	Std. Dev.	
A	pH		Numeric	2	7	-1	1	4.5	1.714986	
B	M	mg	Numeric	5	15	-1	1	10	3.429972	
C	Contact time	min	Numeric	10	50	-1	1	30	13.71989	
Response	Name	Units	Obs	Analysis	Minimum	Maximum	Mean	Std. Dev.	Ratio (max/min)	Model
Y1	RP	%	17	Polynomial	36	95	59.47059	17.9	2.58	Quadratic

Table 2 displays various statistical metrics, including Standard Deviation, R-Squared, Adjusted R-Squared, Predicted R-Squared, and Press, for four distinct models: linear, 2FI, quadratic, and cubic. As indicated by the information in Table 2, the quadratic model (as described in Equation 3) exhibits superior performance, with an R-Squared value of 0.99 and a Predicted R-Squared value of 0.94, outperforming the other models. Nevertheless, it's worth noting that the Predicted R-Squared value can be further enhanced by incorporating machine learning computations.

284 **Table 2. The curve fitting regression outcomes in different mathematical models.**

Source	Std. Dev.	R-Squared	Adjusted R-Squared	Predicted R-Squared	PRESS	
Linear	7.412232	0.869001	0.838771	0.741765587	1407.955	
2FI	8.351559	0.872074	0.795318	0.409168432	3221.353	
Quadratic	2.339108	0.992975	0.983944	0.942684058	312.5	Suggested
Cubic	2.280351	0.996185	0.98474			

285

286 **RP** = -3.38-2.36* pH+5.82*M + 1.07* Contact time+0.14* pH * M+ 0.015* pH * Contact
287 time+ 7.5E-003* M * Contact time+ 1.12* pH^2-0.29* M^2-0.018* Contact $time^2$
288 (3)

289 The Analysis of Variance (ANOVA) results presented in Table 3 demonstrates that the
290 designed model (Equation 1) is significant with a P-value <0.0001 and the error value in
291 prediction (lack of fit) is insignificant indicating the validity of the equation. Among the three
292 parameters (pH, M, and contact time), pH has the smallest P-value (<0.0001) and largest F-
293 value (842.19). Between the other two factors, the mass of adsorbent has more importance (P-
294 value = 0.0039) that the contact time (P-value = 0.0462).

295 **Table 3. The results of ANOVA practices in this study**

Source	Sum of Squares	Mean Square	F-Value	P-value	
Model	5413.9	601.54	109.9436	< 0.0001	significant
A-pH	4608	4608	842.1932	< 0.0001	
B-M	98	98	17.91123	0.0039	
C-Contact time	32	32	5.848564	0.0462	
AB	12.25	12.25	2.238903	0.1782	
AC	2.25	2.25	0.411227	0.5418	
BC	2.25	2.25	0.411	0.5418	
A^2	207.79	207.79	37.97	0.0005	
B^2	235.26	235.26	42.99	0.0003	
C^2	235.26	235.26	42.99	0.0003	
Residual	38.3	5.47			
Lack of Fit	17.5	5.83	1.12	0.4395	not significant
Pure Error	20.8	5.2			
Cor Total	5452.2				

296 The statistical distribution of results is presented in **Figure 11** (Normal% probability via
297 internally studentised residuals). Based on the results the normality of experimental outputs of
298 the DOE were found to be normal all the data are located within the normal diagram according
299 to the declared scheme. A normally distributed dataset implies that the mean and standard
300 deviation of the data are well-defined, which can aid in the design and optimisation of the
301 system. Additionally, engineers can use this information to make informed decisions about the
302 system, such as setting appropriate tolerances for manufacturing processes or determining the
303 expected variability in system performance. Overall, the normality of the experimental outputs
304 is a useful piece of information for engineers to consider when analysing and designing
305 systems. **Figure 12**(a-c) shows the outcomes of the dual sensitive evaluation of effective
306 experimental factors for adsorption of Hg^{2+} onto GO-CTS-PANI. **Figure 12a** demonstrates the
307 influence of pH and amount of adsorbent on the recovery percentage of Hg^{2+}.

308 The findings suggest that elevating the pH level results in an augmentation of the removal
309 percentage (RP) of Hg^{2+}, reaching its peak effectiveness at around pH 6.5-7. This notable
310 enhancement in RP as pH increases is likely attributed to the deprotonation of functional groups
311 like carboxyl, sulfur, and N-H on the adsorbent, enhancing their interaction with Hg^{2+}
312 (Anirudhan et al., 2015; Gao et al., 2021). Conversely, the lower RP of Hg^{2+} in acidic solutions
313 (pH<5) is linked to the protonation of S-atoms in CTS nanoplates, protonation of hydroxyl
314 groups, incomplete dissociation of carboxylic acid groups (which have pKa values around 5)
315 on GO, and protonation of -NH groups on PANI, leading to electrostatic repulsion between
316 Hg^{2+} ions. Within the pH range of 6–7, Hg^{2+} predominantly exists as $Hg(OH)_2$ (approximately
317 79%) and $HgOH^+$ (approximately 10%) (Anirudhan and Shainy 2015). According to the
318 Pearson rule, interactions are more favourable between hard acids and hard bases, and soft
319 acids and soft bases (Santhana Krishna Kumar et al., 2013). Additionally, considering that
320 neutral molecules are softer acids compared to metal cations, the interaction between Hg^{2+}

species becomes more favourable at higher pH values. Regarding the influence of the parameter "M" on RP, an increase in "M" enhances the RP of Hg^{2+} because it provides more available active sites for interaction with the analyte. However, a further increase in the "M" parameter eventually diminishes the RP, primarily due to the aggregation of the adsorbent (Eftekhari et al., 2020). **Figures 12b** and **12c** depict the effects of contact time, "M," and pH on the RP of Hg^{2+}, with the results showing that an extended contact time leads to an improved RP of Hg^{2+}. **Figure 13** shows the EDX spectrum of GO-CTS-PANI adsorbent after adsorption of Hg^{2+} that shows a peak of the adsorbed Hg^{2+} at 9.9 keV. The obtained results clearly shows that Hg^{2+} ions effectively adsorbed onto the GO-CTS-PANI adsorbent.

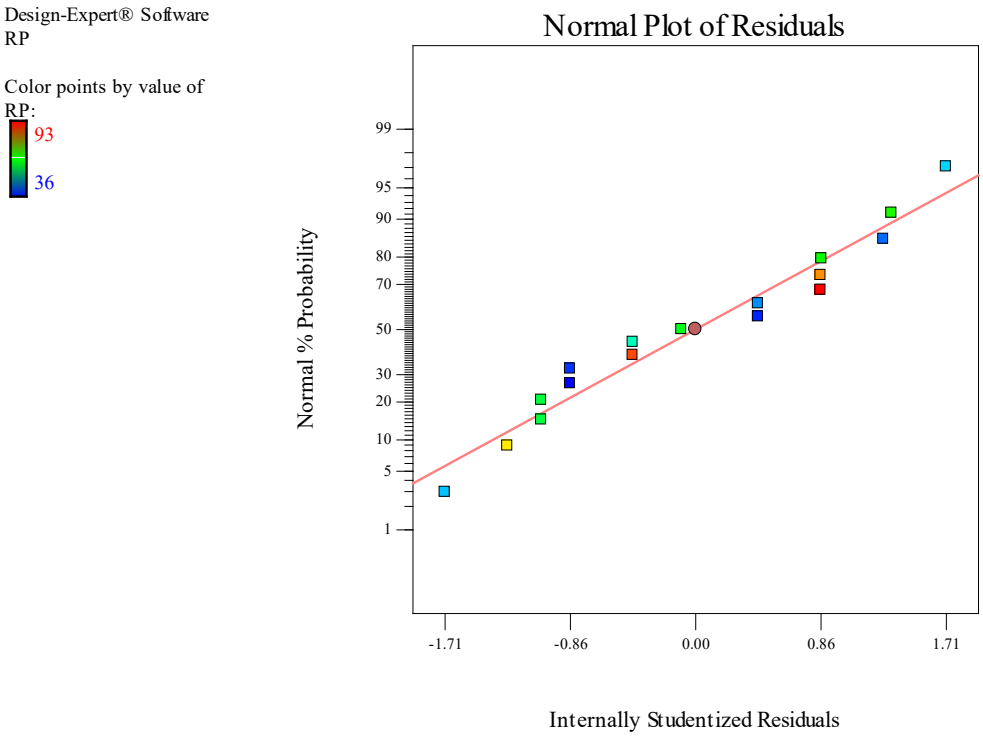

Figure 11. The normal distribution of experimental outcomes in this study

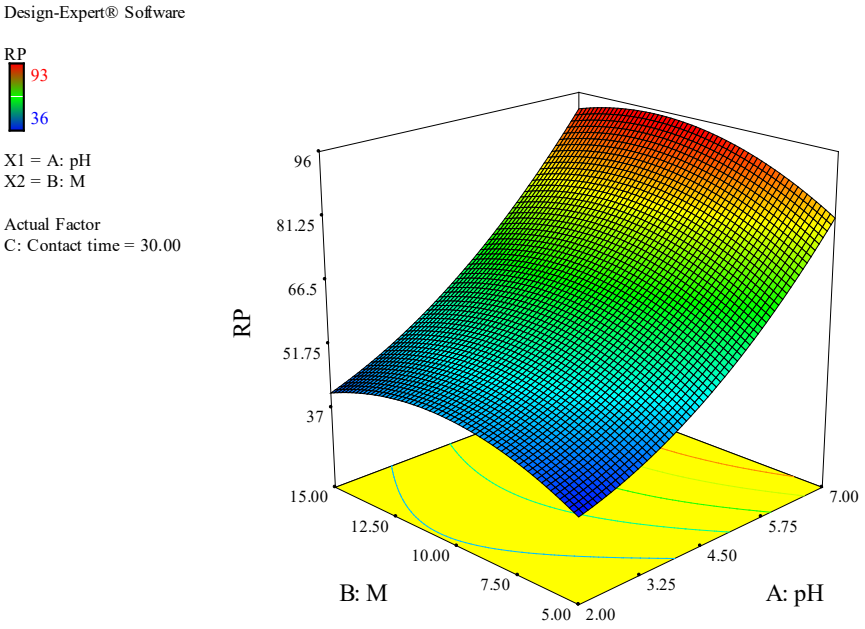
Design-Expert® Software
RP
93
36
X1 = A: pH
X2 = B: M
Actual Factor
C: Contact time = 30.00
RP
96
81.25
66.5
51.75
37
15.00
12.50
10.00
7.50
5.00
B: M
2.00
3.25
4.50
5.75
7.00
A: pH

(a)

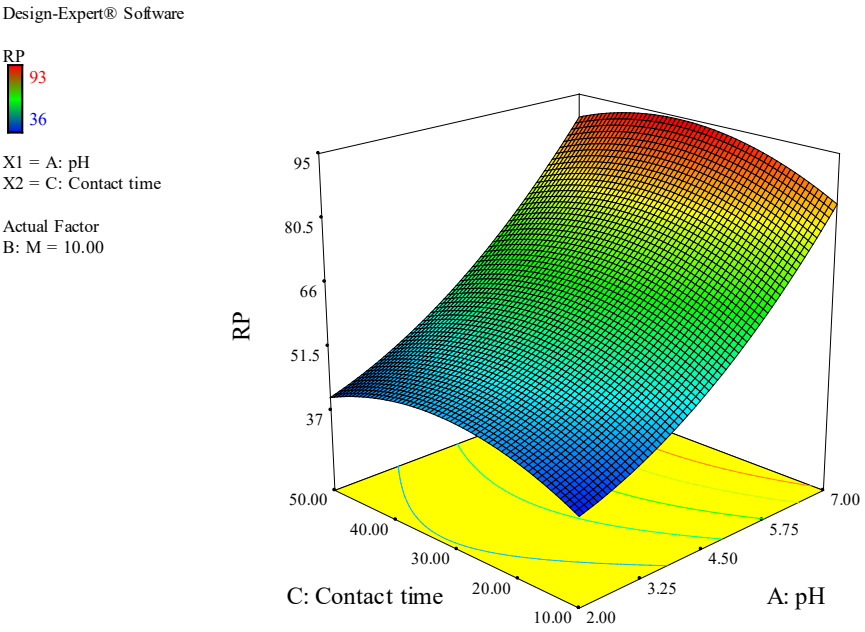
Design-Expert® Software
RP
93
36
X1 = A: pH
X2 = C: Contact time
Actual Factor
B: M = 10.00
RP
95
80.5
66
51.5
37
50.00
40.00
30.00
20.00
10.00
C: Contact time
2.00
3.25
4.50
5.75
7.00
A: pH

(b)

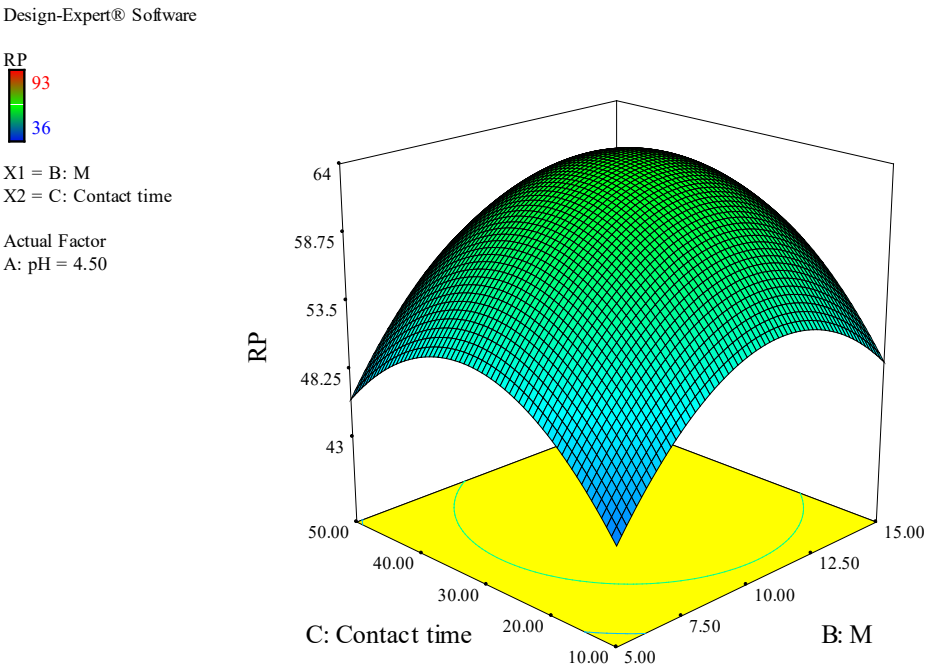

(c)

Figure 12. The sensitive analysis of the studied parameters on RP of Hg^{2+} (50 mg L^{-1}) (a-c).

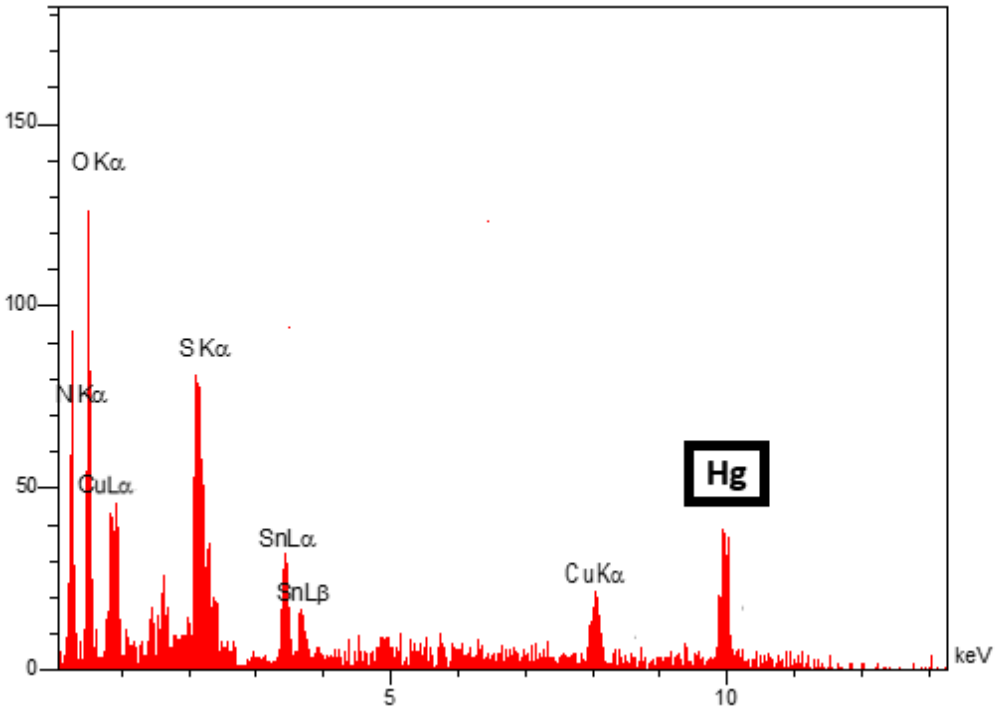

Figure 13. EDX analysis of GO-CTS-PANI after adsorption of Hg^{2+} ions.

After conducting sensitive analysis and mathematical modelling using Box-Behnken model, the optimal values of the effective factors are computed. The results (Table 4) show that the maximum performance (removal percentage as RP) for removing Hg^{2+} from water samples using GO-CTS-PANI is 95%, indicating the best operational efficiency. Therefore, the optimal performance can be obtained based on optimal features of pH of 6.5, M=12 mg and contact time of 30 min. These effective features are also depicted in **Figure 14** based on the desirability. The contours in the figure show that the maximum desirability for predicting the optimal conditions is achieved with high levels of pH and intermediate values of M.

Table 4. The optimal suggestions of effective features based on RP% in this study.

pH	M (mg)	Contact time (minutes)	RP (%)	Desirability
6.59	10.39	40.59	97	1.000
6.56	10.42	39.18	97.6633	1.000
6.50	12.07	30.38	98.3089	1.000

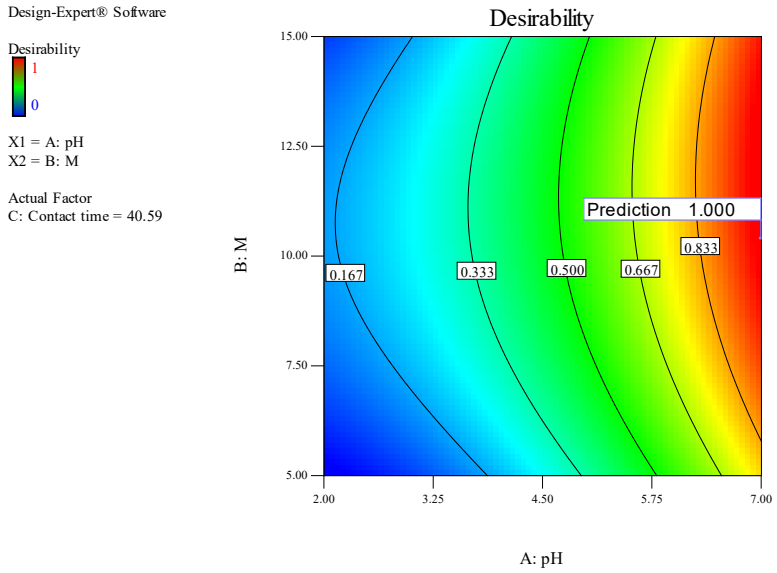

Figure 14. The contours of desirability fluctuations

Adsorption mechanism

Figure 15 shows the mechanism of Hg^{2+} adsorption onto the GO-CTS-PANI adsorbent. The figure shows that there are three main interactions between adsorbent and Hg^{2+} ions, which include: (1)- electrostatic interaction between dissociated carboxylic acid groups of GO and $HgOH^{+}$ ions (Awad et al., 2020) (2)- soft–soft interaction between Hg^{2+} and sulfur atoms of CTS (Anirudhan et al., 2015; Gao et al., 2021; Santhana Krishna Kumar et al., 2013) and (3)- chelating interaction between N and Hg^{2+} (Zeng et al., 2019).

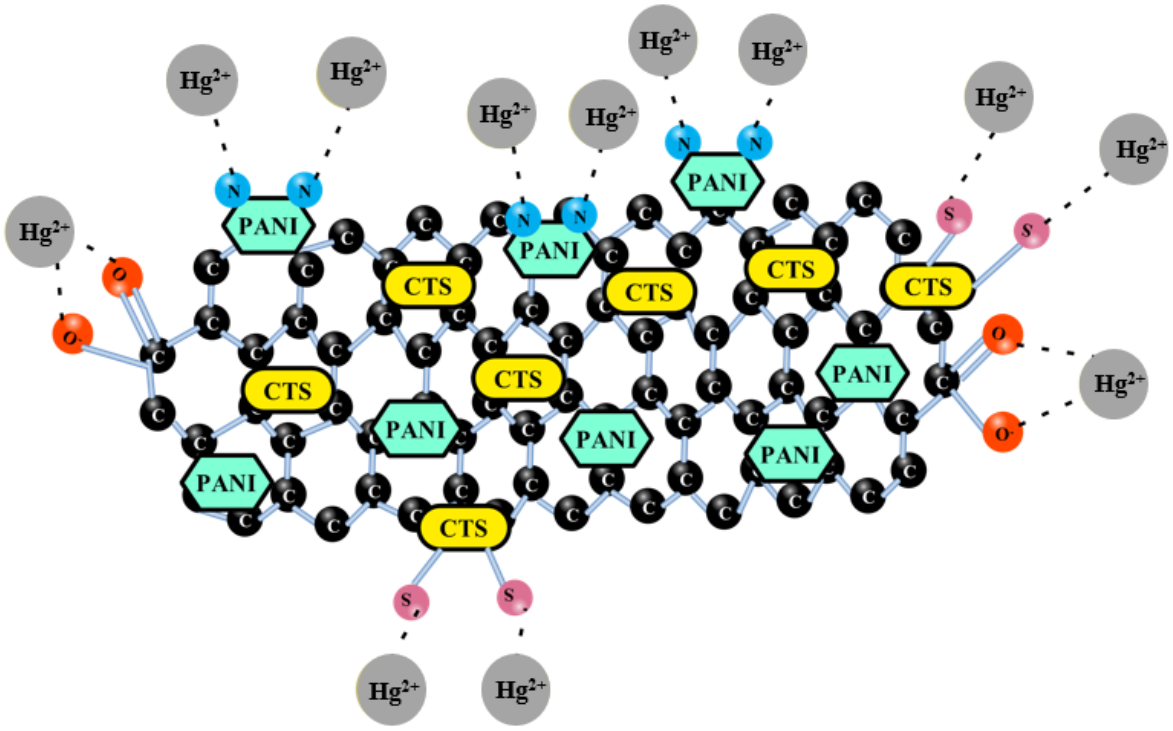

Figure 15. Adsorption mechanism of Hg^{2+} on to the GO-CTS-PANI

Adsorption isotherm

To evaluate the adsorption mechanism and determine the dominance of Freundlich and Langmuir isotherms, two-parameter, and three-parameter equations (mentioned in **Figure 16**) were applied. In the first step, two-parameter calculations are analysed as shown in **Figure 16**.

375 The outcomes indicate that the regression coefficient of both isotherms was over 0.95 and the
376 precise determination of the mechanism is simply not possible. Based on two-parameter
377 relationships, the maximum absorption capacity (Q_{max}), Langmuir coefficient (K_{ads}), K_f and n
378 were estimated as 232.5 mg g^{-1}, 6.76 L mg^{-1}, 32.95 and 1.75, respectively. However,
379 considering the three-parameter Sips, Khan and Toth isotherms (R^2 more than 0.99) and
380 modelling them in Curve Expert Professional software, it was revealed that the exponential
381 coefficients of the models did not converge to 1. Consequently, the Freundlich isotherm was
382 found to be superior (Eftekhari et al., 2020; Eftekhari et al., 2021). It was observed that Hg^{2+}
383 ions were adsorbed onto GO-CTS-PANI in some sequential layers and $0<1/n<1$ indicating a
384 favourable adsorption process. **Figure 17** shows that in Temkin model, b<8 KJ mol^{-1}, and
385 according to the Dubinin-Radushkevich (D-R) equations, E<8 KJ mol^{-1}. Therefore, the
386 adsorption of Hg^{2+} ions onto GO-CTS-PANI is physically in nature. The D-R isotherm model
387 was used to calculate the Q_m and K factors which were found to be 102 mg g^{-1} and 2E-07,
388 correspondingly (Eftekhari et al., 2020).
389

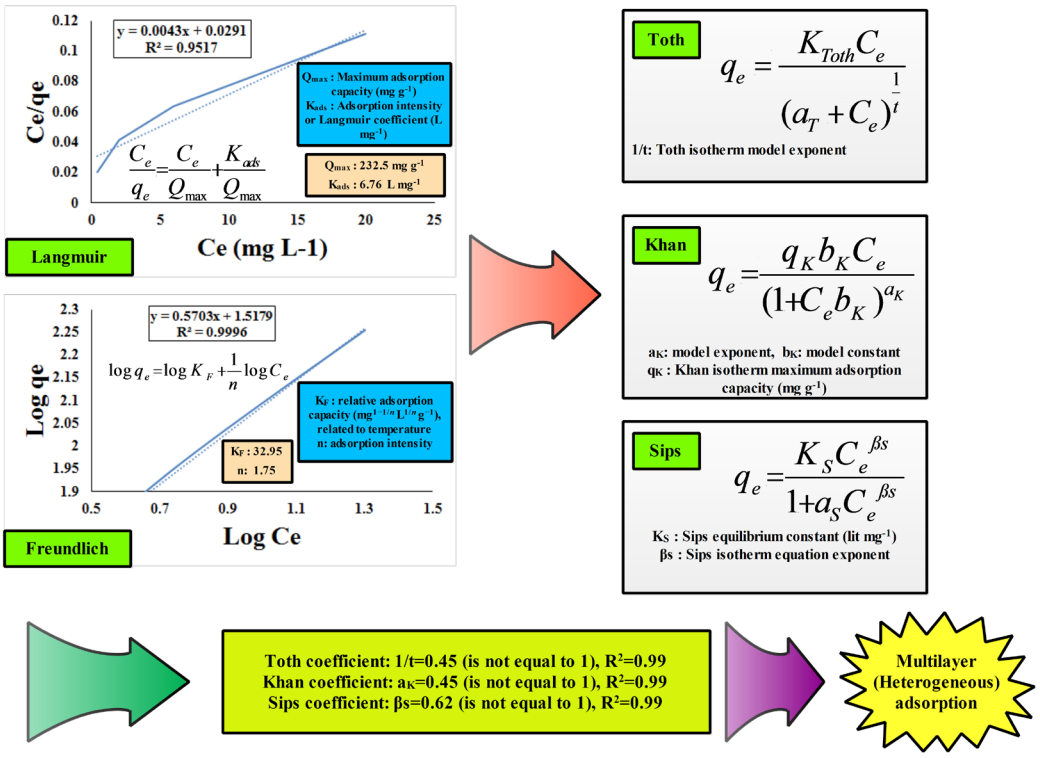

Figure 16. The computational model of Hg^{2+} adsorption onto GO-CTS-PANI.

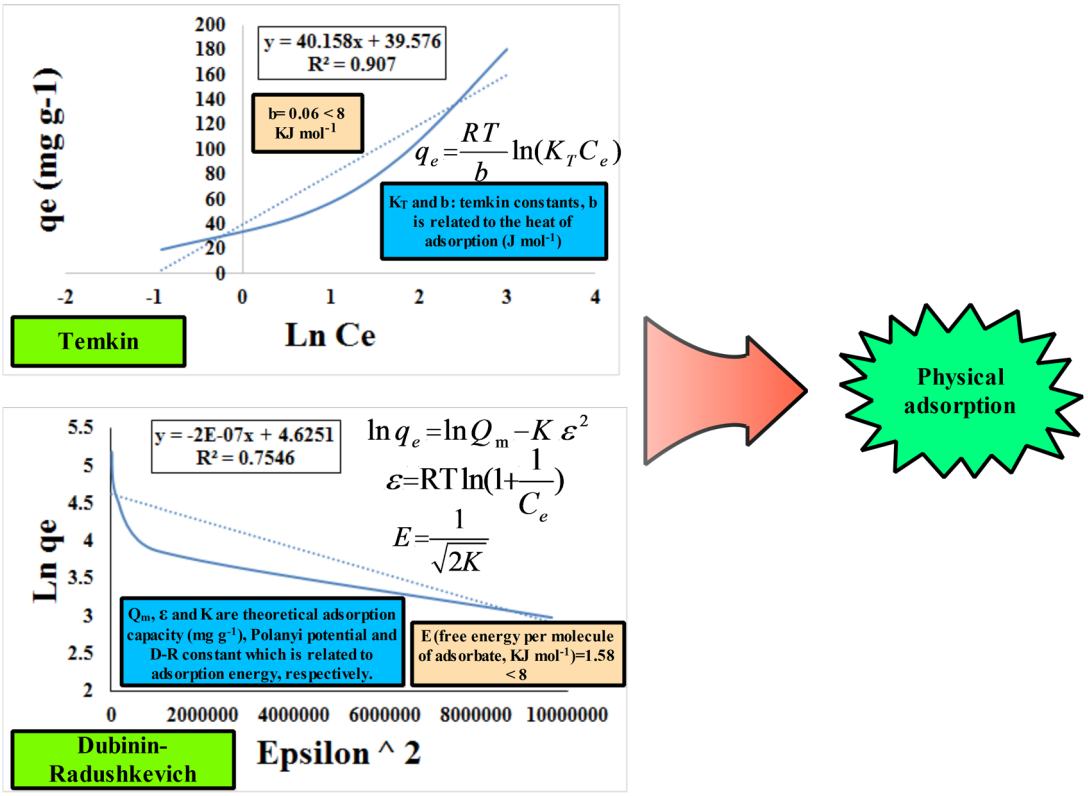

Figure 17. The physical, chemical, or intra-particle mechanism of Hg^{2+} adsorption onto GO-CTS-PANI.

Adsorption kinetic

Figures 18 and **19** demonstrate the results of Hg^{2+} kinetic adsorption onto GO-CTS-PANI using four models: Pseudo-First-Order (PFO), Pseudo-Second-Order (PSO), Intra-particle, and Elovich. Based on the data presented in **Figure 18**, the PSO model produced a more desirable R^2 value and a smaller difference between experimental and calculated q_e values compared to the PFO model. Therefore, it can be concluded that the adsorption of Hg^{2+} onto the GO-CTS-PANI follows by the pseudo second order model with a rate of k_2=0.02 mg g^{-1} min^{-1} (R^2=0.95) (Eftekhari et al., 2020; Eftekhari et al., 2021).

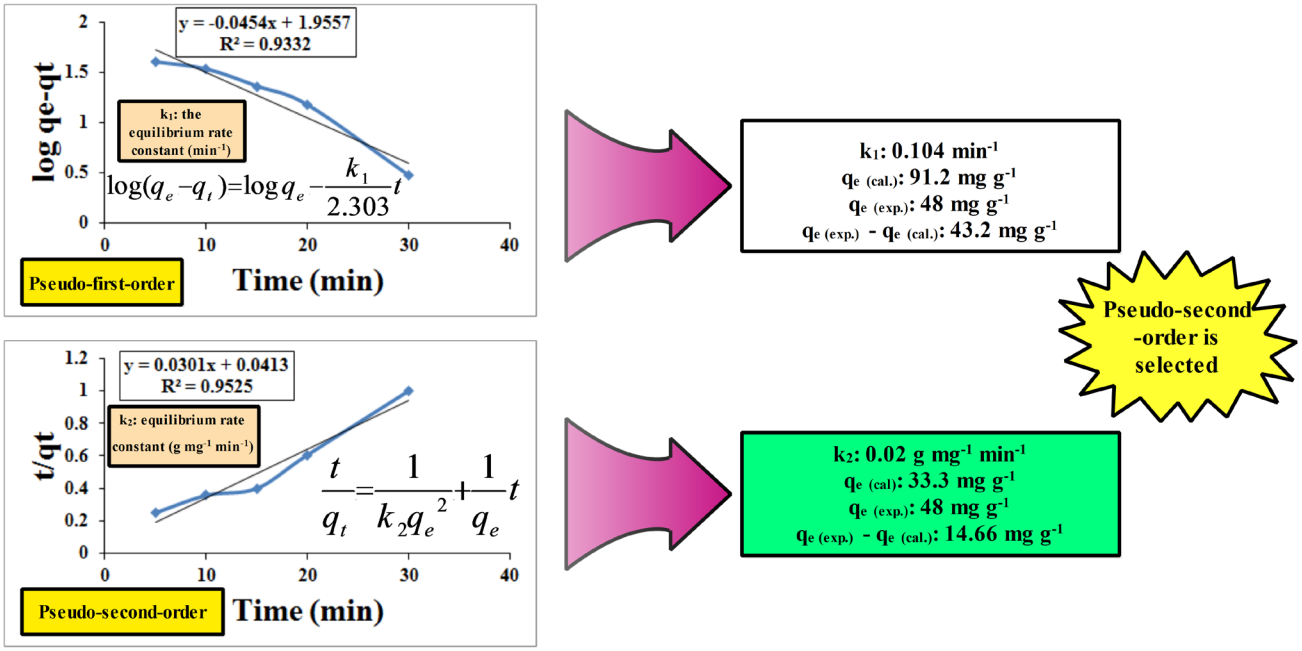

Figure 18. The outputs of kinetic reaction order and coefficient calculations in this study

Figure 19 shows that it is evident that the kinetic behaviour of Hg^{2+} adsorption onto GO-CTS-PANI can be described by both Intra-particle (R2=0.98) and Elovich (R^2=0.94) models. The Intra-particle kinetic curve has intercept of C=-20.6 indicating that both integrated intra-particle and mass transfer mechanisms play a significant role in the adsorption process

(Eftekhari et al., 2020). Moreover, the Elovich model suggests that GO-CTS-PANI has a heterogeneous surface which is consistent with the results of isothermal assessments.

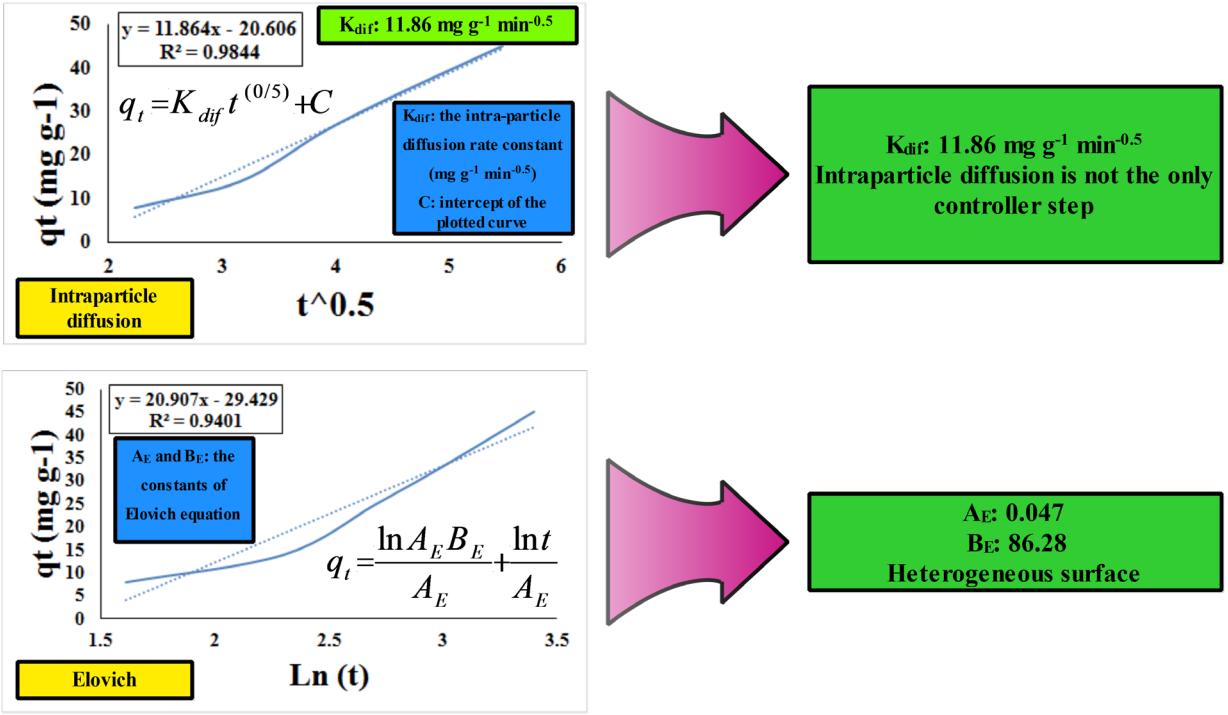

Figure 19. The outcomes of Elovich and Intra-particle kinetic models in the investigation.

Machine learning

This study also utilised machine learning practices for two purposes: (1) to improve the accuracy of prediction parameters and (2) to establish an intelligent infrastructure for online investigation of purification systems using the adsorption method. The distribution of data used in the machine learning process, carried out using the RF method is illustrated in **Figure 20**.

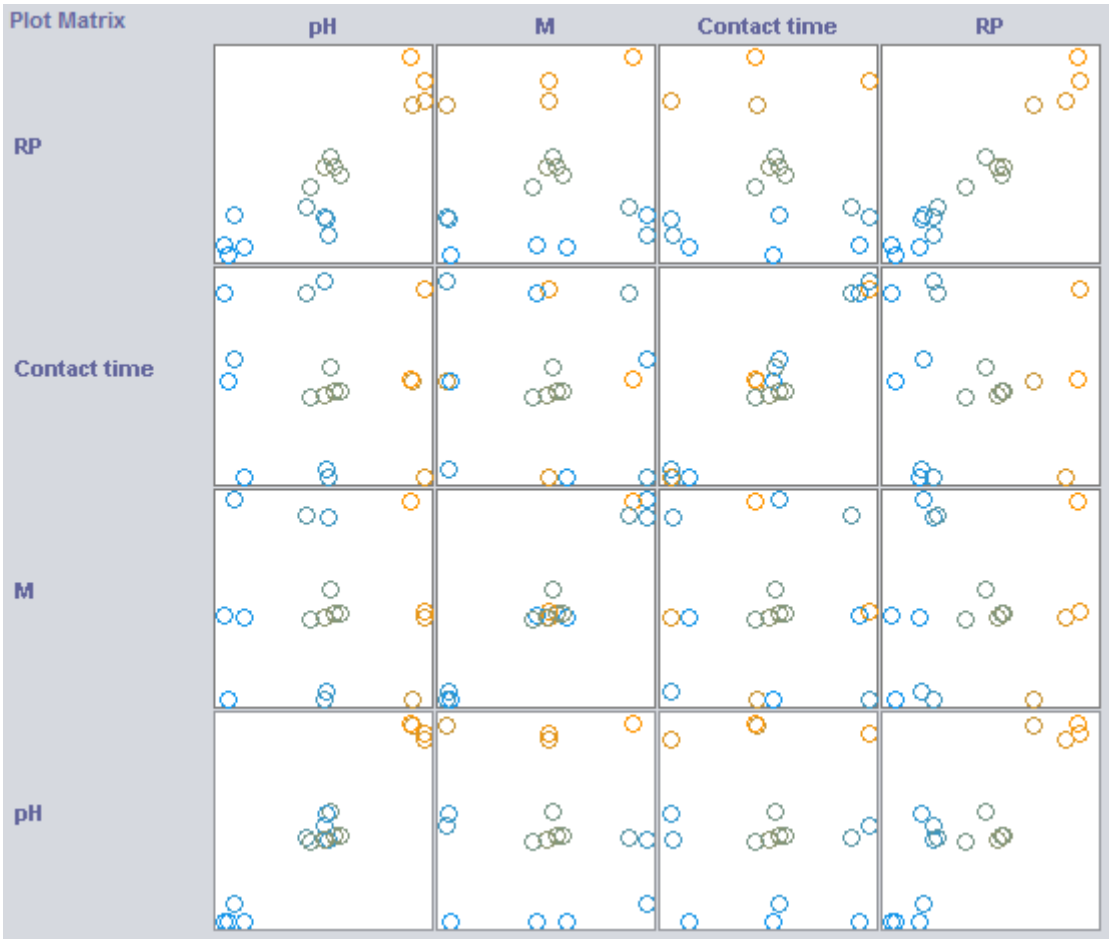

Figure 20. The distribution of data used for the machine learning modelling in this study.

Figure 21 displays the performance of the RF algorithm at different K-Folds Cross-Validation (KFCV) during training and testing process of the data. By adjusting the number of folds, the proportion of testing and training data can be determined. The correlation coefficient (**Figure 21a**) and root mean square error (**Figure 21b**) both indicate that the correlation coefficient generally increases as the number of folds increases but with some fluctuations in different steps. conversely, the behaviour of root mean square error is similar to correlation coefficient but in reverse. Therefore, the best condition is achieved at K=12 and the details are summarised in Table 5. It is worth noting that by applying the RF algorithm, the prediction performance is improved, and operation of the adsorption process can be managed automatically without the need for further examinations or other mathematical computations.

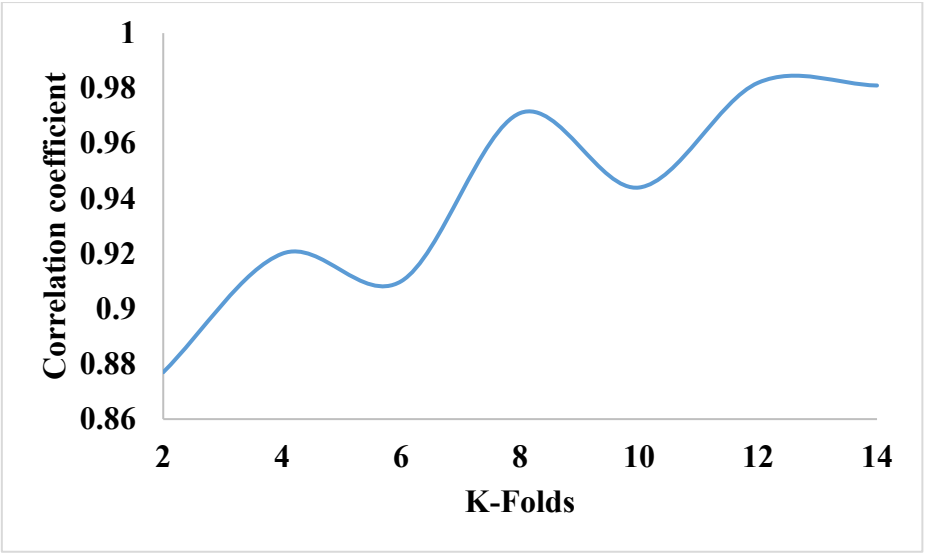

(a)

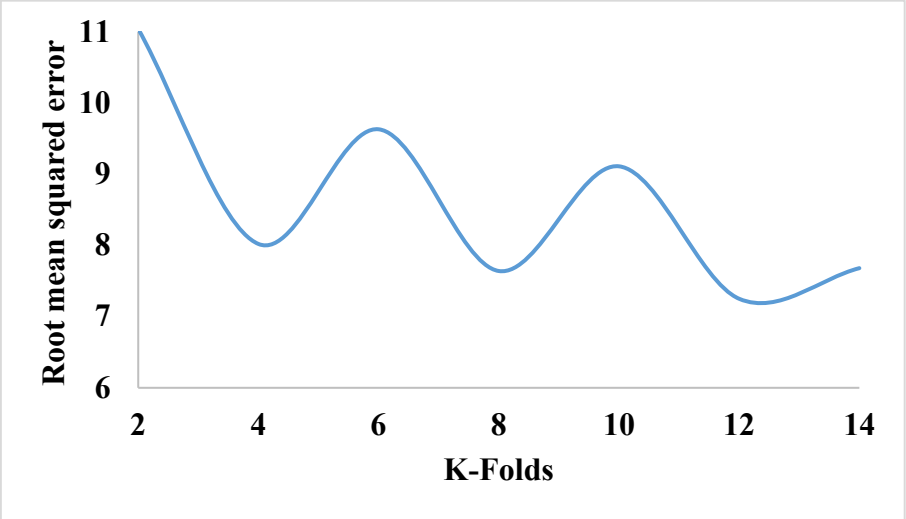

(b)

Figure 21. The effects of the number of K-folds on (a) correlation coefficient and (b) root mean square error

Table 5. The statistical indicators of the RF algorithm performance for K=12

Correlation coefficient	98.2%
Mean absolute error	6.16
Root mean square error	7.25
RAE	38.7%
RRSE	38.26%
Total Number of Instances	17

Figure 22 show the scatterplot between observed and predicted values of the removal percentage (RP). It shows that the prediction process achieved high accuracy, providing evidence of the high validity of the RF algorithm for optimising the adsorption of Hg^{2+} ions onto GO-CTS-PANI nanocomposite. The development of a Decision Support Ssystem (DSS) for the prediction of Hg^{2+} purification from water resources by adsorption process is an important achievement, and the statistical outputs of the system are highly encouraging.

The system employs the RF algorithm and takes into account critical input variables, including contact time, the quantity of adsorbent, and pH. The notably high correlation coefficient of 98.2% signifies a robust positive connection between the input variables and the outcome variable, which, in this instance, pertains to the extent of Hg^{2+} removal. This strong correlation coefficient indicates that the input variables possess substantial predictive power regarding the outcome variable, a crucial characteristic of a dependable Decision Support System (DSS). Mean Absolute Error (MAE) and Root Mean Square Error (RMSE) represent two common metrics for gauging the accuracy of a prediction model. MAE reflects the average absolute disparity between predicted and actual values, while RMSE signifies the square root of the average squared difference between predicted and actual values. In this scenario, the MAE of 6.16 and the RMSE of 7.25 indicate that the DSS's predictions closely align with the actual values. These low values underscore the high precision and reliability of the system's predictions, a vital aspect for effective decision-making.

Furthermore, Relative Absolute Error (RAE) and Root Relative Square Error (RRSE) serve as supplementary metrics for assessing prediction model accuracy. RAE quantifies the average absolute discrepancy between predicted values and actual values, normalized by the average actual value, while RRSE denotes the square root of the average squared difference between predicted values and actual values, also normalized by the average actual value. In this context, the RAE of 38.7% and the RRSE of 38.26% are relatively elevated. This implies that there

exists some degree of error in the DSS's predictions. Nevertheless, it is essential to note that these values still fall within an acceptable range and do not diminish the overall reliability of the system.

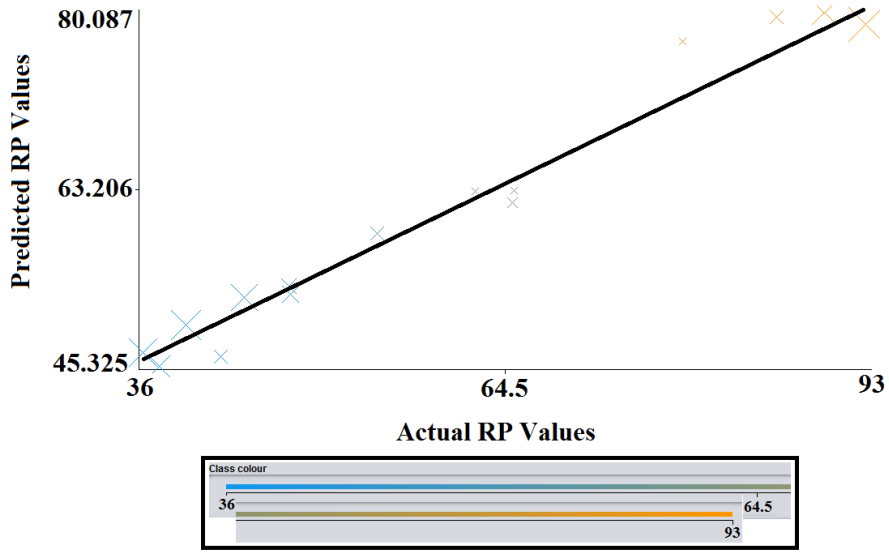

Figure 22. The scatter plot between predicted and actual values of RP% in RF algorithm (K=12)

Test of Reusability

To evaluate the potential for reusing GO-CTS-PANI, we conducted five cycles of adsorption and desorption, employing a 0.1 mol L^{-1} HCl (hydrochloric acid) solution for desorption. As depicted in **Figure 23**, following three rounds of utilizing the GO-CTS-PANI adsorbent, we observed only a marginal 6% decrease in removal percentage (RP). Nevertheless, in subsequent cycles, a more substantial reduction in RP became evident. Based on these observations, it can be inferred that GO-CTS-PANI remains effective for up to three cycles without a noteworthy decline in RP.

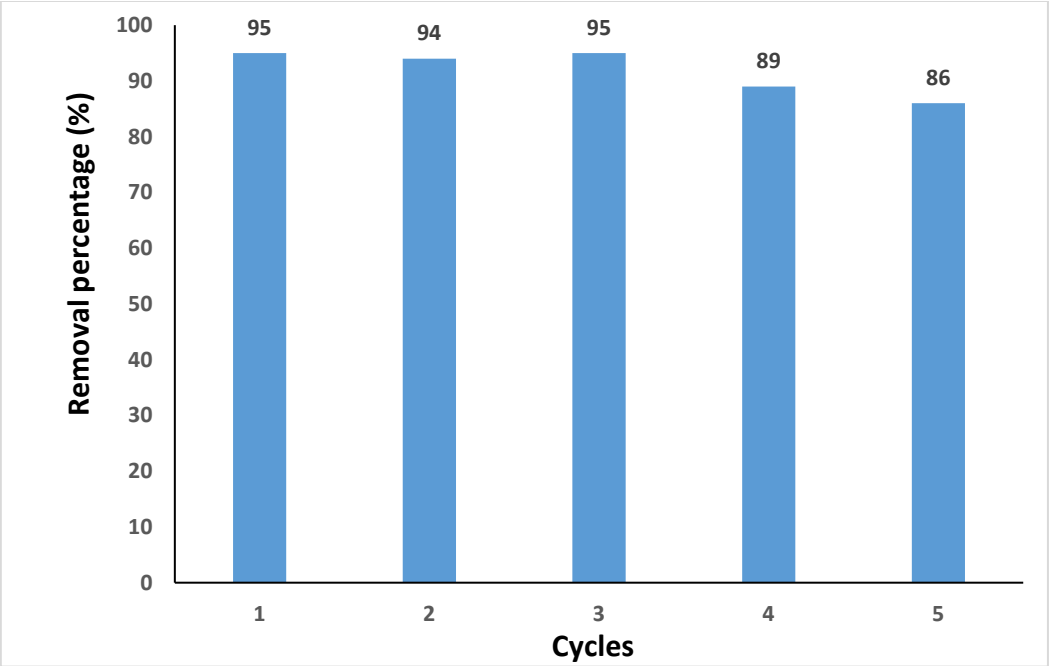

Figure 23. Results of the reusability of GO-CTS-PANI nanocomposite

Comparison with other studies

Table 6 provides a comparison between the newly developed GO-CTS-PANI composite in this study and other adsorbents employed for Hg^{2+} removal. The findings clearly illustrate that this novel adsorbent exhibits a remarkable adsorption capacity for Hg^{2+} within a short timeframe. Furthermore, as it can be effectively reused for at least three cycles without a significant reduction in removal percentage, the GO-CTS-PANI composite can be considered a highly efficient adsorbent. According to the data in Table 6, it is evident that the GO-CTS-PANI composite outperforms other adsorbents, such as palm shell activated carbon modified with ionic liquids, in terms of adsorption capacity. This enhanced performance of the GO-CTS-PANI composite can be attributed to its advantageous functional groups, including the sulfur atoms found in CTS nanoplates, the presence of nitrogen atoms in PANI, and the electrostatic

interactions between the carboxylic acid groups of GO and Hg^{2+} ions. Consequently, these results strongly suggest that GO-CTS-PANI holds substantial promise as a material for effectively removing mercury from aqueous solutions.

Table 6. Comparison between GO-CTS-PANI and other adsorbents for Hg^{2+} removal

Adsorbent	Adsorption capacity (mg g-1)	Reference
2-mercaptobenzamide modified itaconic acid-grafted-magnetite nanocellulose composite	240.0	(Anirudhan and Shainy 2015)
Palm shell activated carbon impregnated with task-specific ionic-liquids	83.3	(Abu Ismaiel et al., 2013)
Polyamine modified reduced graphene oxide	63.8-59.9	(Yap et al., 2020)
Magnetic carbon nanotube	172.8	(Homayoon et al., 2017)
Mercapto-modified bentonite	19.3	(Sahan et al., 2018)
Mercaptobenzothiazole modified cellulose	204.1	(Krishna Kumar et al., 2013)
GO-CTS-PANI	232.5	This study

Conclusions

The GO-CTS-PANI composite proved effective as an adsorbent for eliminating Hg^{2+} from water samples. The optimal conditions, resulting in a 95% removal rate for 50 mg L^{-1} Hg^{2+}, were determined as follows: pH= 6.5, 12 mg of GO-CTS-PANI adsorbent, and a 30-minute contact period, employing the Box-Behnken method. The adsorption process exhibited a multilayer adsorption mechanism with physical interactions on the surface, as evident from conventional calculations. Kinetic analysis revealed that the adsorption reaction adhered to the PSO equation. Sensitivity analysis identified pH as the most influential factor impacting the adsorption process. Both RSM and machine learning techniques, specifically the RF method, proved effective for optimizing the adsorption process and predicting its efficiency, respectively. Furthermore, the GO-CTS-PANI nanocomposite demonstrated its reusability through five cycles of adsorption/desorption, with merely a 6% reduction in removal efficiency observed after three cycles. Ultimately, this study underscores the exceptional efficiency and

reusability of the GO-CTS-PANI composite as an adsorbent for Hg^{2+} removal, showcasing its potential for future applications in water purification.

References

Abu Ismaiel A, Kheireddine Aroua M, Yusoff R (2013) Palm shell activated carbon impregnated with task-specific ionic-liquids as a novel adsorbent for the removal of mercury from contaminated water. Chem Eng J 225: 306-314.

Amini-Fazl MS, Barzegarzadeh M, Mohammadi R (2021) Surface Modification of Graphene Oxide with Crosslinked Polymethacrylamide via RAFT Polymerization Strategy: Effective Removal of Heavy Metals from Aqueous Solutions. J Inorg Organomet Polym 31: 2959–2970.

Albatrni H, Qiblawey H, El-Naas MH (2021) Comparative study between adsorption and membrane technologies for the removal of mercury. Sep Purif Technol 257: 117833.

Anirudhan TS, Shainy F (2015) Effective removal of mercury(II) ions from chlor-alkali industrial wastewater using 2-mercaptobenzamide modified itaconic acid-grafted-magnetite nanocellulose composite. J Colloid Interface Sci 456: 22-31.

Arshad F, Selvaraj M, Zain J, Banat F, Abu Haija M (2019) Polyethylenimine modified graphene oxide hydrogel composite as an efficient adsorbent for heavy metal ions. Sep Purif Technol 209: 870-880.

Awad FS, AbouZied KM, Abou El-Maaty WM, El-Wakil AM, Samy El-Shall M (2020) Effective removal of mercury(II) from aqueous solutions by chemically modified graphene oxide nanosheets. Arab J Chem 13: 2659-2670.

538 Berg DM, Djemour R, Gütay L, Zoppi G, Siebentritt S, Dale PJ (2012) Thin film solar cells
539 based on the ternary compound Cu2SnS3. Thin Solid Films 520: 6291–6294.

540 Briffa J, Sinagra E, Blundell R (2020) Heavy metal pollution in the environment and their
541 toxicological effects on humans. Heliyon 6: e04691.

542 Eftekhari M, Akrami M, Gheibi M, Azizi-Toupkanloo H, Fathollahi-Fard AM, Tian G (2020)
543 Cadmium and copper heavy metal treatment from water resources by high performance
544 folic acid-graphene oxide nanocomposite adsorbent and evaluation of adsorptive
545 mechanism using computational intelligence, isotherm, kinetic, and thermodynamic
546 analyses. Environ Sci Pollut Res 27: 43999-44021.

547 Eftekhari M, Gheibi M, Azizi-Toupkanloo H, Hossein-Abadi Z, Khraisheh M, Fathollahi-Fard
548 AM, Tian G (2021) Statistical optimization, soft computing prediction, mechanistic and
549 empirical evaluation for fundamental appraisal of copper, lead and malachite green
550 adsorption. J Ind Inf Integr 23: 100219.

551 Gao P, Lei J, Tan J, Wang G, Liu H, Zhou L (2021) Self-assembled magnetic microcrystalline
552 cellulose/MoS2/Fe3O4 composite for efficient adsorptive removal of mercury ions (Hg^{2+}).
553 Compos Commun 25: 100736.

554 Ghadirimoghaddam D, Gheibi M, Eftekhari M (2023) Graphene oxide-cyanuric acid
555 nanocomposite as a novel adsorbent for highly efficient solid phase extraction of Pb2+
556 followed by electrothermal atomic absorption spectrometry; statistical, soft computing and
557 mechanistic efforts. Inter J Environ Anal Chem 103:469-490.

558 Global Mercury Assessment 2018. United Nation, Environmental Programme. **2019**.

559 Han Z, Guo Y, Yang W, Tang R, Wang H, Wu S (2020) Removal of mercury from flue gases
560 over iron modified activated carbon made by in situ ion exchange method. J Energy Inst
561 93: 1411-1418.

562 Homayoon F, Faghihian H, Torki F (2017) Application of a novel magnetic carbon nanotube
563 adsorbent for removal of mercury from aqueous solutions. Environ Sci Pollut Res 24:
564 11764–11778.

565 Jathar SB, Rondiya SR, Jadhav YA, Nilegave DS, Cross RW, et al., Ternary Cu2SnS3:
566 Synthesis, Structure, Photoelectrochemical Activity, and Heterojunction Band Offset and
567 Alignment. Chem Mater 33(6): 1983–1993.

568 Lei Y, Chen F, Luo Y, Zhang L (2014) Synthesis of three-dimensional graphene oxide foam
569 for the removal of heavy metal ions. Chem Phys Lett 593: 122-127.

570 Li L, Luo C, Li X, Duan H, Wang X (2014) Preparation of magnetic ionic
571 liquid/chitosan/graphene oxide composite and application for water treatment. Int J Biol
572 Macromol 66: 172-178.

573 Liu J, Duan Y, Song L, Zhang X (2018) Constructing sandwich-like polyaniline/graphene
574 oxide composites with tunable conjugation length toward enhanced microwave
575 absorption. Org Electron 63, 175-183.

576 Mbanga O, Ncube S, Tutu H, Chimuka L, Cukrowska E (2019) Mercury accumulation and
577 biotransportation in wetland biota affected by gold mining. Environ Monit Assess 191:
578 186.

579 Krishna Kumar AS, Kalidhasan S, Rajesh V, Rajesh N (2013) Adsorptive Demercuration by
580 Virtue of an Appealing Interaction Involving Biopolymer Cellulose and
581 Mercaptobenzothiazole. Ind Eng Chem Res 52: 11838–11849.

582 Raj D, Maiti SK (2019) Sources, toxicity, and remediation of mercury: an essence review.
583 Environ Monit Assess 191: 566.

584 Rezazadeh N, Danesh S, Eftekhari M, Farahmandzadeh M (2022a) Application of graphene
585 oxide and its derivatives on the adsorption of a cationic surfactant (interaction mechanism,
586 kinetic, isotherm curves and thermodynamic studies). J Mol Liq 368: 120720.

587 Rice KM, Walker EM, Wu M, Gillette C, Blough ER (2014) Environmental Mercury and Its
588 Toxic Effects. J Prev Med Public Health 47(2): 74–83.

589 Saadati T, Eftekhari M, Rezazadeh N, Nazarabad MK (2023) Graphene oxide–bismuth
590 tungstate (GO–Bi2WO6) nanocomposite as a green adsorbent for lead removal: isotherm,
591 kinetics and thermodynamic study. Int J Environ Sci Technol 20: 1301–1314.

592 Sahan T, Erol F, Yilmaz S (2018) Mercury(II) adsorption by a novel adsorbent mercapto-
593 modified bentonite using ICP-OES and use of response surface methodology for
594 optimization. Microchim J 138: 360-368.

595 Santana AJ, dos Santos WNL, Silva LOB, das Virgens CF (2016) Removal of mercury(II) ions
596 in aqueous solution using the peel biomass of Pachira aquatica Aubl: kinetics and
597 adsorption equilibrium studies. Environ Monit Assess 188: 293.

598 Santhana Krishna Kumar A, Kalidhasan S, Rajesh V, Rajesh N (2013) Adsorptive
599 Demercuration by Virtue of an Appealing Interaction Involving Biopolymer Cellulose and
600 Mercaptobenzothiazole. Ind Eng Chem Res 52: 11838-11849.

601 Shabani-Nooshabadi M, Zahedi F (2017) Electrochemical reduced graphene oxide-polyaniline
602 as effective nanocomposite film for high-performance supercapacitor applications.
603 Electrochim Acta 245: 575-586.

Streets DG, Devane MK, Lu Z, Bond TC, Sunderland EM, Jacob DJ (2011) All-Time Releases of Mercury to the Atmosphere from Human Activities. Environ Sci Technol 45: 10485–10491.

Tchounwou PB, Ayensu WK, Ninashvili N, Sutton D (2003) Environmental exposure to mercury and its toxicopathologic implications for public health. Environ Toxicol 18(3): 149-75.

Vasudevan S, Lakshmi J, Sozhan G (2012) Optimization of electrocoagulation process for the simultaneous removal of mercury, lead, and nickel from contaminated water. Environ Sci Pollut Res 19: 2734–2744.

Velempini T, Pillay K (2019) Sulphur functionalized materials for Hg(II) adsorption: A review. J Environ Chem Eng 7: 103350.

Wang C, Tian H, Jiang J, Zhou T, Zeng Q, He X, Huang P, Yao Y (2017) Facile Synthesis of Different Morphologies of Cu2SnS3 for High-Performance Supercapacitors. ACS Appl. Mater. Interfaces 9 (31): 26038–26044.

Wei Y, Zhang Y, Gao X, Ma Z, Wang X, Gao C (2018) Multilayered graphene oxide membranes for water treatment: A review. Carbon 139: 964-981.

Yan X, Feng J, Li P, Li J, Ren B, Gao S, Cao R (2021) Fast and efficient removal of mercury ions using zirconium-based metal–organic framework filter membranes. Inorg Chem Commun 131: 108796.

Yap PL, Tung TT, Kabiri S, Matulick N, Tran DNH, Losic D (2020) Polyamine-modified reduced graphene oxide: A new and cost-effective adsorbent for efficient removal of mercury in waters. Sep Purif Technol 238: 116441.

626 Yu JG, Yue BY, Wu XW, Liu Q, Jiao FP, Jiang XY, Chen XQ (2016) Removal of mercury by
627 adsorption: a review. Environ Sci Pollut Res 23: 5056–5076.

628 Zaman MB, Poolla R (2020) Morphological tuning of hydrothermally derived visible light
629 active Cu2SnS3 nanostructures and their applications in photocatalytic degradation of
630 reactive industrial dyes. Opt Mater 104: 109853.

631 Zeng H, Wang L, Zhang D, Yan P, Nie J, Sharma VK, Wang C (2019) Highly efficient and
632 selective removal of mercury ions using hyperbranched polyethylenimine functionalized
633 carboxymethyl chitosan composite adsorbent. Chem Engin J 358: 253-263.

634
635
636
637
638
639
640
641
642
643
644
645
646
647
648

Ethical approval

Not applicable.

Consent to participate

Not applicable.

Consent for publication

Not applicable.

Competing interests

The authors declare no competing interests.

Contributions

Sara Enferadi: data curation, methodology; Mohammad Eftekhari: data curation, methodology, supervision, conceptualization, writing—review and editing; Mohammad Gheibi: methodology, software, writing—review and editing; Nikoo Nabizadeh Moghaddam: data curation, methodology; Stanislaw Wacławek: writing—review and editing, and supervision; Kourosh Behzadian: data curation and conceptualization, supervision, writing—review and editing.

Funding

There is no funding for this research.